Optimization and Inverse Design of Floor Tile Airflow Distributions in Data Centers Using Response Surface Method

Long Phan, Beichao Hu, Cheng-Xian Lin[†], and George S. Dulikravich*

Department of Mechanical and Materials Engineering, Florida International University, 10555

W. Flagler St., EC 3445, Miami, FL 33174, United States

*Multidisciplinary Analysis, Inverse Design, Robust Optimization and Control (MAIDROC) Laboratory

ABSTRACT

Computational fluid dynamics (CFD) has become a popular tool compared to experimental measurement for thermal management in data centers. However, it is very time-consuming and resource-intensive when used to model large-scale data centers, and often unrealistic for real-time thermal analyses. In addition, it is prohibitive to use CFD for optimization process where thousands of designs need to be generated. Floor tile airflow distribution control is a key technique for maintaining a sufficient cold air delivery to variable thermal loadings of server cabinets. Regular practice of deploying a set of identical floor tiles may not result in the best solution for airflow uniformity through tiles. In this paper, an optimization procedure based on response surface methodology (RSM) is proposed to find the best arrangement of mixed-porosity floor tiles for different targeted tile airflow distributions. Fast-approximation RSM based on radial basis

---

† Corresponding author: Cheng-Xian Lin. Email: lincx@fiu.edu. Phone: +1 (305) 348-0537

function (RBF) allows thousands of designs to be generated for the optimization process which uses genetic algorithm as its main solver. The method shows proven success in maximizing floor tile airflow uniformity, and in the inverse design optimization where various tile airflow distribution topologies, i.e., linear, parabolic, and sinusoidal shapes are targeted. For the considered data center and aisle configuration, the improvement over the all-uniform-tile design is 55% in terms of standard deviation to the average tile airflow rate, whereas 90%, 91%, and 94% in root mean square error (RMSE) for the linear, parabolic, and sinusoidal floor tile airflow distribution objectives, respectively.

Keywords: Computational fluid dynamics, response surface, radial basis function, optimization, data center, tile modeling, tile airflow uniformity

1. INTRODUCTION

Recent advances in information technology (IT) have offered new capabilities for internet users to innovate and achieve more via telecommunication, internet of things, and cloud computing. Service providers are motivated to expand more businesses and provide better services to their users. This causes a high demand in power density within server racks inside a data center. One of the common thermal problems in data centers is the air recirculation between the hot aisle and cold aisle. In an open aisle data center, the ratio of floor tile-to-server airflows is an important factor for regulating this phenomenon; however, in an aisle containment data center, the level of segregation between hot and cold aisles plays an important role in the magnitude of recirculation. Kumar and Joshi [1] experimentally studied the effects of floor tile-over-server rack flow ratios, and were able to point out the locations of air recirculation by varying floor tile flow rates. Sharma et al. [2] proposed supply and return heat indices (SHI and RHI) to evaluate the hot and cold air mixing issues previously mentioned.

Tile airflow distribution plays an important role in regulating the air mixing issue and hot spots in IT equipment. Performance and durability of computer servers are very much dependent on the management of these hot spots. In an open aisle configuration, the air profile in front of server racks is much influenced by floor tile airflow distribution. When deploying a set of uniform floor tiles with the same porosity, non-uniformities in tile airflow are often encountered. The level of airflow uniformity depends on many factors, e.g., the raised floor depth, the size of a data center, or the distance from a computer room air handling (CRAH) unit to the layout position of perforated tiles. Since tile airflow has a direct impact on server racks, the need for controlling the floor tile airflow distribution is of importance in data centers. For better understanding of the cause of non-uniformity in floor tile airflow, VanGilder and Schmidt [3] studied airflow uniformity through

FE-20-1718   Lin

perforated tiles in 240 CFD data center models. They concluded that perforated tile type and the

presence of plenum obstructions have the greatest potential influence on airflow uniformity. Type

of perforated tiles used such as ones with different porosities and plenum obstruction such as

cables, stanchions, pipes, etc. account for the pressure loss across the raised-floor plenum. In fact,

these two major sources indicate the vital role of pressure loss in regulating the tile airflow

distribution. Therefore, by controlling the pressure loss, one can obtain a nicely uniform

distribution through perforated tiles. This is attainable either by adjusting the tile porosity or having

the plenum obstruction arranged in a certain way to achieve the airflow uniformity. For better

understanding of plenum obstructions, VanGilder et al. [4] studied a compact stanchion model by

introducing the loss coefficient which can reduce the computational overhead and is easy to specify

in CFD tools. Fulpagaree et al. [5] studied the effect of plenum chamber obstructions and

concluded that up to 80% in air flow rate decrease and up to 2.5ºC increase in temperature are

caused by such obstructions. The situation involving plenum obstruction is usually very

complicated and not easy to control due to the layout of the plenum construction, e.g., piping

systems, cables, stanchions, etc. Perhaps, a more manageable way to deal with the airflow non-

uniformity is through tile selection and arrangement. Phan et al. [6] studied different mixed tiles

arrangement to remedy the airflow non-uniformity caused by various layout positions of the

CRAH unit in a small data center model.

Computational fluid dynamics (CFD) programs are excellent numerical tools for studying

airflow and heat transfer models in data centers. These models give good predictions and useful

insights while eliminating the expensive cost of performing experiments. A few selected recent

studies of whole data center scale using CFD as the key numerical tool can be referred in [7], [8],

[9], [10]. These studies demonstrate the advantages of using CFD analysis to predict the thermal

profile in various data center layouts. Some other multi-scale data centers such as [11], [12], [13], [14], [15] also rely on CFD tool to guide their research. Detailed studies of data centers are computationally prohibitive due to various small features such as tiny pores in perforated tiles. Therefore, in recent years, researchers have focused on developing more simplified tile models for data centers [16], [17], [18], [19]. Among these tile models, the modified body force model [18] is the most advanced one in capturing the velocity field right after tiles.

Optimization is a very powerful tool for the design of data centers, especially in the early design stages. A good selection of different equipment including CRAH units, perforated tiles, server racks, etc. can save much money for business owners. Decision on choosing the right equipment to save energy depends upon the results from optimization study of various design parameters. Indeed, optimization study needs to be carried out prior to new construction of a data center to avoid unwanted facility reconstruction due to ineffective utilization of energy. Optimization study requires an objective function to be optimized, and this function can be formulated easily through a mathematical model of various input parameters. However, when a mathematical model is not available, experiments or simulations are then the options to represent for such objective functions. For instance, Egorov-Yegorov & Dulikravich [25] relied on several experiments in an optimization study to achieve a superalloy from various chemical elements. Li et al. [23] relied on computational method by coupling Proper Orthogonal Decomposition (POD) model with genetic algorithm for an optimization study of a ventilation system inside an office. Many design objectives are sought to be minimized including fan power, CO_2 concentration, cooling energy requirement. During an optimization process when a direct mathematical model of the objective function is not available, designs need to be prepared either through experiments or simulations. However, experiments are normally limited due to high operational costs, and

FE-20-1718   Lin

simulations based on CFD are very time-consuming. Therefore, it is very difficult or even unfeasible for generating thousands of design parameters in an optimization process.

Response surface methodology (RSM) is in essence a multi-dimensional data fitting method used to approximate empirical data. RSM relates several independent input variables to an output known as a response. The process is relatively fast and computationally efficient, therefore, RSM is usually employed during an optimization process to generate multiple virtual designs without the need for all of the high-cost computational analyses. RSM was first introduced by Box and Wilson [28] back in 1951. RSM has recently gained popularity in many applications including sheet metal forming [24], chemical composition of new superalloys [25], and improved RSM for faster engineering application approximations [26], [27]. RSM can provide useful accurate information while using less computational resource. In recent studies, Colaço & Dulikravich have developed the RSM-based hybrid optimizer capable of interpolate both linear and non-linear functions in multi-dimensional spaces with up to 500 dimensions [29], [30], [31]. They also performed an in-depth comparison of various deterministic and stochastic optimization techniques, as well as RSM technique in complex high dimensionality problems [32]. These studies are particularly useful for many inverse design engineering applications with highly accurate and small computing time. Among the methods for constructing an RSM model, radial basis function (RBF) is more preferable as a basis function to construct response surfaces due to its high accuracy, yet less mathematical computing effort. The use of RBFs followed by collocation is a technique first proposed by Kansa [33] after the work of Hardy [34] on multivariate approximation. RSM does not require a large data set to train the response surface. In fact, it can work with a sparse data set to interpolate more extra points (virtual data points). One advantage while using RSM is the ability to extrapolate reasonably accurate information outside the domain of interest within less

than 5% of the original dataset [35]. In regard to data center or building research, RSM has not

extensively been explored. Phan and Lin [36] attempted to use RSM to optimize various design

input parameters, as well reconstructed the airflow and temperature fields of a data center model

[35]. The latter research is potentially useful for real-time thermal monitoring of data centers.

Since the optimal distribution of supply air flow rate through perforated tiles is among the

key concerns in regard to the thermal management in data centers, in this paper, the authors

introduce the RSM-based optimization procedure to find the optimum arrangement of mixed tiles

for various tile airflow distributions. By selecting the right floor tiles, data center management

team is equipped with the right tool in the first step to tackle the bigger problem, hotspots in

server racks. This indirectly opens a whole new possibility for thermal dynamic control of server

rack, especially in occasion where a temporary change in rack thermal load may require special

air distribution profiles. By inverse design powered by RBF model, one can achieve different

flow profiles through porosity control of floor tile. Relying on CFD simulation for thousands of

designs during an optimization is impractical or prohibitive. Therefore, through its rapid RBF-

based approximation, RSM was used to accommodate thousands of virtual designs during the

optimization process. However, some initial CFD-based designs were required to train the

response surfaces. The CFD simulation results used in this paper relate to the same data center

model that were well-validated in the literature [1], [18], [19], [20]. In the first part of the paper,

the RSM approach is demonstrated with the objective of seeking the best tile porosity arrangement

that can create a uniform airflow distribution through perforated tiles. In the second part of the

paper, a prescribed airflow distribution of choice is obtained through the inverse design

optimization, and three different scenarios including linear, parabolic, and sinusoidal tile airflow

distributions are achieved with success. In data center thermal management, airflow uniformity

across server racks is generally preferred to sufficiently provide cold air for server racks at uniform loading. However, in some scenarios where variable loadings are presented in some server racks, various airflow distribution tweaks to direct more cold air to some hottest server racks and less air in other servers with less intensive loading. By demonstrating different airflow profiles (such as linear, sinusoidal, etc.) with corresponding floor tile solutions, the authors would like to address the ability to use RBF model to achieve this goal quickly. This could be particularly useful for modern data centers, which commonly undergo different non-uniform thermal loadings among server racks. For the zones that are adjacent to more thermal loading racks, they require a higher level of cooling, thus, more floor-tile airflow. In fact, as more advanced tiles with greater flexibility in porosity control are currently in use, the study could inform best practice in regard to perforated tiles placement to control more suitable tile airflows depending on thermal loading, and therefore, a more energy-efficient data center can be achieved.

Nomenclature

$\widehat{m}$	Predicted tile mass flow rate [kg/s]
$\bar{\dot{m}}$	Average tile mass flow rate [kg/s]
$\dot{m}$	Simulated tile mass flow rate [kg/s]
$\dot{M}$	Objective function
$\hat{y}$	Predicted value
$\bar{y}$	Mean value
c	Shape parameter
L	Number of variables
n	number of values
P	Number of input variables or points
r	Distance [m]
R^2	R-squared
$S(P)$	Series of points

STD	Standard deviation
T	Tile porosity [%]
W	Weight matrix
x	x coordinate
y	y coordinate or observed value

Subscripts

i	i^{th} index
L	L^{th} index

Greek symbols

ξ	Approximation function
Ξ	Approximation function matrix
ϕ	Basis function
Φ	Basis function matrix

2. CFD MODELING

2.1 Data center model description

The data center model used in this paper is modeled after the *Data Center Laboratory (DCL)* at Georgia Tech which also used in previous studies [1], [18], [19]. The dimension of the data center model in L × W × H is 28.5 ft. × 21.3 ft. × 8.5 ft. (8.7 m × 6.2 m × 2.6 m). Three CRAH units placed in the room extend from the floor all the way to the ceiling. CRAH 1 & 2 are down-flow units while CRAH 3 is the only up-flow unit. However, in this study, only CRAH 1 was utilized, and other two were blocked off. Two additional units with an equal height of 5.68 ft. (1.73 m) placed in the room are the power distribution unit (PDU) and the coolant delivery unit (CDU). The standard 42U server racks are filled with four 10U rack-mounted server simulators. Each

9

FE-20-1718   Lin

server simulator model has a dimension of 24 in. (60.96 cm) wide, 18 in. (45.72 cm) high, and 27.125 in. (69 cm) deep. There is a 6 in. (15.24 cm) gap at the foot of the server rack.

The server racks are arranged in such a way that the front-door sides facing each other form a cold aisle. This cold aisle is where the two rows of standard 2×2 ft^2 perforated tiles are positioned to supply cooled air to the server racks. The back sides of the server racks exhaust heat from active servers by internal fans to form hot aisles as seen in Fig. 1. The underfloor plenum has a height of 3 ft. (0.91 m), which is relatively deep to ensure airflow velocity is normal to the floor tiles. The ceiling plenum height is 3 ft. (0.91 m). The ceiling vents are located along the walls of the hot aisle sides (refer to Fig. 2).

2.2 Computational Model

The computational domain of the current data center model is shown in Fig. 2. The downflow CRAH unit number one was aligned with the middle of the cold aisle was modeled as a black box, i.e., only mass flow inlet was specified at the bottom surface of the CRAH assuming no leaking anywhere in the raised floor and a constant system static pressure in the CRAH. The other two CRAH units were not considered in this study, and therefore, only serves as space fillers. The supply airflow from CRAH unit number one was assumed to be normal to the surface of discharge. The ceiling vents were treated as pressure outlets with a zero-gauge pressure. There are totally 8 server racks arranged in two rows with 4 server simulators per rack as seen in Fig. 1, and each server was modeled as a black box. Since there are total 4 server racks in each row and 4 server simulators in each rack, both the front and back sides of each row were divided in 16 smaller windows representing 16 server simulator cabinets. Server rack thermal load is not considered in this study because only airflow modeling is investigated. Due to the nature of a black box model, thirty-two small surfaces facing the cold aisle were treated as outflow, while 32 exhaust surfaces

FE-20-1718   Lin

facing the hot aisles were modeled as inflow. The perforated floor tile flow model used was the modified body force model with a six-inch enhanced momentum region above and normal to all eight perforated tiles. This tile model has extensively been validated with high fidelity [18], [19]. The three-foot raised floor plenum was included in the domain without any stanchions, pipes, or cables explicitly modeled, while the ceiling plenum was not modeled.

2.3 Numerical Model

Standard k-ε turbulence model [37] was utilized in the numerical process using ANSYS Fluent [40]. Majority of the wall adjacent cells have mesh satisfying $y+ > 30$ while fine near-wall grids were adopted for much smaller $y+ < 5$. Therefore, enhanced wall treatment was deployed to ensure numerical stability for a wider range of mesh, with most of the near-wall cells of $y+ \sim 1$. The total mesh size was optimized at 1.7 million cells with mostly hexahedral meshes. The convergence criteria were set to be less than 10^{-4} in residuals for all computed variables within less than 1% difference of the quantity of interests within the entire domain. Since only airflow simulation is performed, the energy equation was not solved in this study. The gradients in spatial discretization were selected as least square cell based. The pressure-velocity coupling scheme used was the SIMPLE algorithm. Second order upwind scheme was used for momentum, while first order upwind scheme was used for turbulent kinetic energy and turbulent dissipation rate equations.

Since the server rack model consisted of mostly orthogonal features, it was therefore meshed with a cut-cell method where hexahedral mesh is dominant. Grid independence study was performed to ensure an accurate result yet less computing time. Three mesh sizes include coarse, medium, and fine were studied. The Grid Convergence Index (GCI) was calculated based on the maximum velocity at the centerline of the perforated tile 5 through 8 (refer to Fig. 1). The grid

FE-20-1718   Lin

convergence was found to be within the asymptotic range of convergence with ~1.010946581. It

was found that at 1.7 million cells, the integrity of the tile velocity was preserved, and a further

increase in grid size would not justify more computing time.

3   RESPONSE SURFACE METHODOLOGY (RSM)

3.1 Fundamentals of RSM

Response surface methodology often starts with a database of training designs to construct

for a response surface that fits through these designs by using an algorithm to guess the value of

the unknown function on the basis of an assumption such as regularity, physical meaning, and

statistical variability. RSM estimates the combination of the input parameters yielding an optimal

response through fast-running approximation of the simulation process.

Response surface training is based upon a complete dataset, e.g., an evaluated design of

experiment (DOE) information, experimental data, simulated results, etc. to create an

approximation of the response in the design space. In this paper, high-fidelity Heat Transfer/CFD

simulation data was used for training the response surface which was used later in the optimization

procedure. Response surfaces are advantageous in problems where limited information is

provided. However, the results obtained from these hyper-surfaces may be inaccurate if the design

space exploration is poor and if an unsuitable method is chosen. Normally, the higher the number

of training designs, the more accurate will be the RSM model. Furthermore, the design dispersion

in the design space should be as uniform as possible for training a response surface.

3.2 Radial Basis Function (RBF)

Some of the optimization techniques that may require thousands of objective functions

calculation, and the objective functions may require hours or days to complete. Therefore, if one

relies on traditional mesh-based methods, the calculations will be prohibitive due to the cost of

time required. The need for a simplified model or a metamodel that represent the original problem

is indeed necessary. For instance, by using kernel interpolation/approximation technique, response

surface methods which are based on linear and non-linear regression and other variants of the least

square technique can be used to reduce a significant amount of time for those problems. These

methods are often regarded as mesh-free methods.

One of the most popular mesh-free kernel approximation techniques uses radial basis

functions (RBFs). Initially, RBFs were developed for multivariate data and function interpolation.

It was found that RBFs were able to construct an interpolation scheme with favorable properties

such as high efficiency, good quality and capability of dealing with scattered data, especially for

higher dimension problems.

The radial basis functions typically have the following form

$$S(\boldsymbol{P}) \cong \xi(\boldsymbol{x}) = \sum_{i=1}^{N} w_i \phi(r) \tag{1}$$

where $P=\{P_1,...,P_i,...,P_L)$ and $S(\boldsymbol{P})$ is known for a series of points $\boldsymbol{P}$. The approximating function

$\xi(\boldsymbol{x})$ is represented as a sum of N radial basis functions, $\phi(r)$, where $r = |\boldsymbol{x} - \boldsymbol{x}_i|$. Each RBF is

associated with a different center $\boldsymbol{x}_i$, and weighted by an appropriate coefficient, w_i. The weights

w_i can be computed by using the matrix methods of linear least squares. Since the values of $\boldsymbol{P}$

points are known, they can be substituted and eq. (1) is now rewritten in the matrix form.

$$\boldsymbol{\Phi} \, \boldsymbol{W} = \boldsymbol{\Xi} \tag{2}$$

where unknowns are the weight matrix $\boldsymbol{W}$, and $\boldsymbol{\Phi}$ & $\boldsymbol{\Xi}$ are the basis and approximation function

matrices, respectively. Once all the weights are known, they can be put back into eq. (1) to obtain

FE-20-1718   Lin

the approximate function $\xi(x)$. In order to solve for the weight matrix, W, from eq.(2), matrix Φ needs to be inverted as shown in eq.(3).

$$W = \Phi^{-1}\Xi \qquad (3)$$

In multi-dimensional problems, r is the distance between two points. RBFs are special functions that have a finite value for $r = 0$, and tends to zero as r goes to infinity. These functions are called globally supported. Some of the globally supported RBFs used in this paper are shown in eqns. (11) – (14) of Table 1. The shape parameter c_j is kept constant as 1/N. It is used to control the smoothness of the RBF. Fig. 3 shows the influence on its choice for the *multiquadrics* RBF. An increase in c results in a smoother curve for RBF.

3.3 RSM Performance Criteria

RSM accuracy depends on several factors such as the complexity of the variations of the solution, the number of points in the original DOE and the choice of the type of RSM. Since an RSM model is typically obtained through an approximation process, it is very important to assess its quality with respect to the available real designs for reasonable accuracy. Multiple RSMs for the same output variable should be created and compared against one another before choosing the best one. If the quality is unsatisfactory, the process should be restarted, and further experiments should be made. In any case the described procedure should be iterated several times in order to obtain the best possible results. To provide a more complete picture of metamodel accuracy, three different metrics are often used: *R-square, Relative Average Absolute Error (RAAE), and Relative Maximum Absolute Error (RMAE)* [38].

R Square

$$R^2 = 1 - \frac{\sum_{i=1}^{n}(y_i - \hat{y}_i)^2}{\sum_{i=1}^{n}(y_i - \bar{y})} = 1 - \frac{MSE}{variance} \tag{4}$$

where, $\hat{y}_i$ is the corresponding predicted value for the observed value y_i; $\bar{y}$ is the mean of the

observed values

While mean square error (*MSE*) represents the deviation of the metamodel from the real

simulation model, the variance captures any irregularities. A larger value of *R-square* indicates a

more accurate metamodel.

Relative Average Absolute Error

$$RAAE = \frac{\sum_{i=1}^{n}|y_i - \hat{y}_i|}{n * STD} \tag{5}$$

where *STD* stands for standard deviation. RAAE shows the relative average absolute error

calculated for *n* values. The smaller the value of *RAAE*, the more accurate the metamodel.

Relative Maximum Absolute Error

$$RMAE = \frac{\max\left(|y_1 - \hat{y}_1|, |y_2 - \hat{y}_2|, \ldots, |y_n - \hat{y}_n|\right)}{STD} \tag{6}$$

Large *RMAE* indicates large error in one region of the design space even though the overall

accuracy indicated by *R-square* and *RAAE* can be very good. Therefore, a small *RMAE* is preferred.

However, since this metric cannot show the overall performance in the design space, it is not as

important as *R-square* and *RAAE*.

3.4 Tile Airflow Uniformity and Inverse Design Optimization

modeFrontier optimization program [41] was used for demonstrating the RSM method.

The optimization was carried out utilizing the genetic algorithms (GAs) based entirely on RSM

for calculation of the generations. GAs are based on the principles of natural genetics and natural

selection. It is suitable for the indoor environment of building optimization since it is a gradient-

FE-20-1718 Lin

free stochastic optimization method [21], [22]. Compared with other stochastic search methods, GAs have the features of robustness and effectiveness even in noisy environments [23]. The basic elements of natural genetics – reproduction, crossover, and mutation – are implemented during numerical optimization. Table 2 summarizes all of the attributes considered during a GA process. The general form of the objective function is shown in eq. (7).

$$\dot{M}(T); \ T = \{T_1, T_2, \cdots, T_L\} \tag{7}$$

where $T_1, T_2, \cdots, T_L$ are the tile porosities, which can be modified in order to find the minimum value of the function $\dot{M}$.

$$\dot{M} = \begin{cases} \sqrt{\dfrac{\sum_{i=1}^{N}(\hat{m}_i - \bar{\bar{m}})^2}{n}}, & uniformity \ design \tag{8} \\ \\ \sqrt{\dfrac{\sum_{i=1}^{N}(\hat{m}_i - \dot{m}_i)^2}{n}}, & inverse \ design \tag{9} \end{cases}$$

In the tile airflow uniformity design optimization, the objective function ($\dot{M}$) is essentially the standard deviation between the predicted tile mass flow rates by RSM, $\hat{m}_i$, and the average value, $\bar{\bar{m}}$. The standard deviation has a direct implication on airflow uniformity along the tiles, which is critical to ensure every server receive enough cold air for a thermally healthy status. By minimizing the standard deviation, a solution for selecting an appropriate floor tile perforation and arrangement is solved. In the inverse design optimization, the objective function ($\dot{M}$) is the root mean square error between the predicted tile mass flow rates by RSM, $\hat{m}_i$, and the CFD values, $\dot{m}_i$. In both cases, n represents the number of tiles.

4 RESULTS AND DISCUSSION

4.1 Tile airflow uniformity optimization

FE-20-1718   Lin

In this section, the objective is to use optimization based on RSM to seek the best distribution in tile porosities that can provide a uniform airflow distribution for all tiles. For achieving this goal, response surfaces associated with four different RBF models (eqs. (11) – (14)) were carefully trained and evaluated. The aim was to search for a suitable RBF corresponding to a response surface training. The reliability of the RBF model and the accuracy of the response surface interpolation depend upon the accuracy obtained through assessment criteria stated in eqs. (4) – (6). Each response surface construction requires a sufficient number of training points. Naturally, the higher the number of training points, the more reliable the response surface. A basic rule for finding the order of magnitude of the necessary training points consists in identifying the minimum number of training points which would be necessary to compute a second order polynomial response surface and considering a number of training points which is about twice that minimum number or at least greater than that minimum. For ensuring a uniform exploration in the range of the input parameter space, the minimum number of training points is calculated as shown in eq. (10). [41]

$$P \geq \frac{(L+k)!}{L!\,k!} \tag{10}$$

where P is the number of training points, L is number of input variables, k is the degree order of polynomial. Therefore, with eight tile porosities input, the minimum number of training point for a second order polynomial response surface is 45 design cases. Due to space limit, only 10 out of 45 designs are shown in Table 3. In order to obtain a good response surface, it is also important that the input parameters space is uniformly explored in the range of variations of the input parameters. In the range of exploration from 10% to 80% tile porosity, Sobol's algorithm [39] was used for the preparation of training design cases. The algorithm provides a random selection of porosity arrangement uniformly distributed in the proposed range of exploration.

FE-20-1718   Lin

After performing the response surface training for four different RBF models, the next step is to assess the credibility of each model. Ideally, if a response surface is able to identify the behavior of the system, the output (standard deviation of the tile mass flow rate) computed by the response surface will coincide with the CFD-simulated values. In Fig. 4, real and virtual points represent CFD-simulated values and the RSM-predicted values, respectively. Both *multiquadrics* and inverse *multiquadrics* RBFs do a good job in predicting the designs. However, out of four RBF models investigated, the values predicted by *multiquadrics* RBF are the closest to the simulated values with smallest difference, while the values predicted by *Gaussians* RBF are the worst in terms of fluctuating distance.

For an assurance of the best RBF model, performance criteria recommended in eq. (4) – (6) were evaluated. The iterative stages were executed to seek a converged result (optimum design), and at each stage validation was performed to ensure the suitable designs are selected to proceed to the next stage. After four stages, a desirable design was achieved with no further stage required since only minimal change was occurred after the fourth stage. As seen in Table 4a, for the first iterative stage of the optimization process, the *multiquadric* RBF (eq. (11)) consistently dominates other RBF models in three performance metrics in terms of *R-squared*, *RAAE*, and *RMAE*. Indeed, it has the highest *R-squared* measurement, lowest *RAAE* and *RMAE*. In the next three iterative stages (Table 4b, c, &d), it is also the *multiquadrics* that stands out as the most suitable RBF model for training the response surface.

Now that the suitable response surface based on the *multiquadrics* RBF is selected, the 3-D response surface is then explored. Because of the limit of space in this paper, only the response surface constructed for the optimization in the 1st iterative design stage is presented. There are also 8 tile porosity inputs, but only the first two tiles are presented. The shape of the 3D response

FE-20-1718   Lin

surface is shown in Fig. 5a, while the projections onto each plane surface are presented in Fig. 5a, b, & c. A marked point is presented in the plots to show how it is located in different 2D perspectives of the 3D surface. Ideally, we want to find the corresponding tile porosities that result in the lowest standard deviation. The point with the smallest standard deviation when observed in all 8 tile porosities then becomes our objective of the problem.

After the suitable response surface was constructed, the optimization process proceeded in searching for the best arrangement of mixed-porosity floor tiles to obtain the minimum total deviation in air flow rates. During one stage, thousands of virtual designs with different tile porosity combinations between 10% - 80% (labeled with t1, t2, …, t8) were generated with GA based entirely on the corresponding trained response surface. These generated designs are all plotted in Fig. 6, and each chart in this figure corresponds to one stage labeled.

A constraint of 0.05 is placed on the standard deviation to highlight the best population at each stage. A few best designs from this population were then selected and validated against the simulated designs. The predicted designs passing the selection test criteria discussed later in this section, were added to the original data set for the next stage of optimization, and the whole process including RSM training and generation of predicted designs by GA was repeated. It was found that after four stages of optimization, the objective for best floor arrangement was reached.

The selection criteria were considered with priority order given as follows: 1) the simulated design value is smaller than the predicted design value, or the difference between predicted and simulated designs is within 10 percent; 2) designs with smallest differences are acceptable. The first criterion is considered because simulated designs with smaller standard deviations help driving the process closer to the desirable solution. If the first criterion cannot be met, then the second criterion helps selecting the closest simulated designs for the next stage of optimization.

FE-20-1718   Lin

At least five simulated designs corresponding to five predicted designs that are selected by the selection criteria were then added to the original dataset for the next stage of optimization including new RSM.

Fig. 7 shows the validation process at the first three stages of the design process. This figure shows that "difference" reduces with increasing number of "stages", which suggests that the entire design process is converging. Fig. 7b, d, and f also shows the mass flow rates for all tiles slowly become flatter throughout the stages. This serves as a basis for the success of the fourth stage when the final design outperforms the original design in standard deviation as shown in Fig. 9a. Although there are eight design cases are validated as each stage, only five good ones are selected to carry on the next optimization stage.

The tile porosity configuration of design cases selected at each stage are shown in Fig. 8. From the mentioned selection criteria, there are five validated designs are selected in the first three stages. The predicted design shown in stage 4 is the final product of the optimization process. The tile porosity arrangement of the final design is varied from 50% – 70%. The final predicted design was also validated and reflected in the simulated design. This design is improved over the original design with all uniform tiles at 56% porosity. (see Fig. 9).

The tile mass flow rate evolution throughout iterative stages of the optimization process is demonstrated in Fig. 9a. Indeed, improvement through stages with respect to the airflow uniform distribution line is observed. Also, the contour plot of the final best design compared with the original design is shown in Fig. 9b. The final design in stage 4 almost reaches the uniformity with a relative improvement in standard deviation of 55% compared to the original design with all tiles at 56% porosity.

4.2 Inverse design optimization

FE-20-1718   Lin

Sometimes, due to the uneven thermal load distribution of server racks within a data center, the demand for supply cool air from perforated tiles are also varied in the cold aisle. Even with a uniform thermal load provision, the server racks that are positioned near the two ends of the perforated tiles rows tend to be hotter compared to the ones in the middle of the tile rows. This is referred to end effect which is well-known in the data center industry. For resolving these issues, the tile airflow needs to be adjusted to overcome these drawbacks. An intentional tile airflow distribution in a specific arrangement is, therefore, the subject in this inverse design optimization.

The idea is to use optimization to pick out the best tile porosity arrangement that satisfies the proposed airflow distribution objective. For demonstrating this concept, three airflow distribution scenarios in tiles are proposed, i.e., the linear, parabolic, and sinusoidal distributions as shown in

Table 5. For all scenarios, the total mass flow rate through all 8 tiles are maintained at 12 kg/s or 20,756 CFM. The respective chart for

Table 5 is plotted in Fig. 10. The next three sections discuss the optimization processes similar to the uniformity design optimization with the objective function is the root mean square error (RMSE) defined in eq. (9). An optimal design in each scenario is reached when the RMSE is less than 5% compared to the proposed airflow distribution curve.

4.2.1 Linear tile airflow distribution

The first scenario of tile airflow distribution is the linear shape with a gradual increase in tile airflow from tile 1 through 8. The optimization process to minimize the RMSE is similar to the uniformity design optimization where iterative stages are deployed to reach the final objective. A response surface was trained in each stage and assisted in the prediction of the designs. Performance measurement was also carried out to ensure the best suitable RBF model used.

FE-20-1718   Lin

Due to the space limit in the paper, all of the charts describing the validation process at each stage can be retrieved from the appendix. Here, only the final designs after validation are presented. Fig. 11 shows the tile porosity for best validated designs at each stage. The validation process is very successful in overall, especially in stage 3 where all of the best designs suggested from the RSM-based optimization. The evolving progress of tile porosity throughout each stage is gradually shaped into a linear arrangement as seen Fig. 11. The final best design is presented in stage 4.

Fig. 12 shows the tile mass flow rate for all best designs at each stage compared to the original and proposed linear airflow distribution designs. Clearly, it is shown that the design presented in stage 4 meets the expectation proposed with only 6% in RMSE compared to the proposed linear distribution. The contour plot in Fig. 12b also confirms the agreement with a relative improvement in RMSE of 90% of the optimized over the original designs when both are compared to the targeted linear airflow distribution line.

4.2.2 Parabolic tile airflow distribution

The whole optimization process for parabolic airflow distribution scenario is also identical to previous scenarios. The final results are shown in Fig. 13, while the validation demonstration can be referred to the appendix. Overall, the progress to the final best design presented in the final stage is very successful. Unlike the uniformity design optimization, the validation is much smoother in the inverse design optimization where many suggested best designs are well-validated and exceed the expectation. The reason is that the original design with uniform tile porosity of 56% has almost uniform airflow distribution in the tiles due to the symmetrical position of the CRAH unit placed in the data room. Therefore, there are little rooms for improvement in that case. For the inverse design optimization, a distinct airflow distribution shape is proposed which

FE-20-1718   Lin

requires many more developments, as a result, the progress in each iterative stage shows a distinct improvement.

The progress to reach the final design that matches the proposed shape is demonstrated in Fig. 14. As expected, the final design in the last stage shows particularly good agreement with the proposed design (RMSE = 6%). The relative improvement of 91% in RMSE of the optimized over the original designs is reflected in Fig. 14b, when both are compared to the proposed parabolic distribution line. Tiles 1 & 8 show the smallest mass flow rate, while tiles 5 & 6 receive the peak airflow rate.

4.2.3   Sinusoidal airflow distribution

Lastly, the sinusoidal airflow distribution shape explored in this section is an extreme condition which the tiles are undergoing an oscillating form of airflow rate. The validation process can be referred to the appendix. Here, the final optimal designs in each iterative stage are observed. Fig. 15 shows best designs selected at each iterative stage.

Fig. 16 shows the progress toward the proposed objective. The best design in stage 4 matches well with the proposed shape with the RMSE only 5.9%. It is also shown that the original design with uniform porosity of 56% cannot create an alternating trend in tile airflow as compared to the optimized design in this work, and Fig. 16b clearly shows this comparison with a relative improvement in RMSE of 94% of the optimized over the original designs, when both are compared to the proposed sinusoidal distribution line.

In addition to reaching all design objectives for both the uniformity design and the three inverse designs, the time required for the optimization processes is also advantageous aspect when using RSM. In fact, if CFD method was to be used instead of relying on the response surfaces, the total time spent for generating all predicted designs during an optimization process takes 9000

FE-20-1718   Lin

hours or 375 days since each simulation costs approximately 2 hours of run time and there are
4500 predicted designs generated with GAs. This is based on a 4-core personal Dell computer with
Intel® Core™ i7-4770 CPU at 3.4 GHz with 32 GB of memory. For a response surface trained at
each iterative stage, the total time for obtaining the predicted designs is only a few seconds.
Overall, the total time required for the entire design process from preparing the original data set to
the complete final design is outlined in Table 6. This proves a substantial time reduction when
using RSM for optimization processes. Moreover, the RSM can be used in conjunction with
experimental testing at each iterative design stage to increase the level of accuracy and fidelity of
the entire design method.

5 CONCLUSIONS

In this research paper, response surface methodology based on radial basis function was
used to aid in an optimization effort to seek an optimal arrangement of mixed-porosity tiles for
either a uniform (uniformity design optimization) or a specific (inverse design optimization) tile
airflow distribution. Details of the RSM-based optimization through iterative stages are
demonstrated including the response surface training, performance assessment, as well as
validation with CFD simulated results. In both the uniformity design and the inverse design
optimization processes, the method successfully suggests better arrangements of mixed-porosity
tiles over the original design of deploying all uniform tiles at 56% porosity in data centers. In fact,
the relative improvement over the original design is 55% in terms of standard deviation in the
uniformity design optimization, whereas it is 90%, 91%, and 94% in RMSE for the linear,
parabolic, and sinusoidal tile airflow distributions, respectively, in the inverse design optimization.
Without relying on CFD method for generating virtual designs, the RSM shows a substantial time
reduction at each iterative stage during an optimization process. With the available tool for tile

FE-20-1718   Lin

porosity adjustment, the method presents an innovative technique that allows better arrangements of mixed-porosity tiles over traditional uniform tiles practice to provide more uniform or targeted cold-air profiles to server racks with or without uniform thermal loadings. As a result, this is very promising for cooling energy saving potential without sacrificing server performance as each server rack can be specifically paired with suitable perforated floor tiles for maximum airflow delivery.

ACKNOWLEDGEMENT

6   REFERENCES

[1]   Kumar, P., & Joshi, Y. (2010) Experimental investigations on the effect of perforated tile air jet velocity on server air distribution in a high density data center. In Thermal and Thermomechanical Phenomena in Electronic Systems (ITherm), 2010 12th IEEE Intersociety Conference on Thermal and Thermomechanical Phenomena in Electronic Systems, Las Vegas, NV, pp. 1-7.

[2]   Sharma, R.K., Bash, C.E. &, Patel, C.D. (2002) Dimensionless parameters for evaluation of thermal design and performance of large-scale data centers. In: Presented at the8th ASME/AIAA Joint Thermophysics and Heat Transfer Conference, St. Louis, MO, pp. 1–11.

[3]   VanGilder, J. W., & Schmidt, R. R. (2005, January). Airflow uniformity through perforated tiles in a raised-floor data center. In ASME 2005 Pacific Rim Technical Conference and Exhibition on Integration and Packaging of MEMS, NEMS, and Electronic Systems

collocated with the ASME 2005 Heat Transfer Summer Conference, San Francisco, CA, pp. 493-501.

[4]   VanGilder, J. W., Pardey, Z. M., Bemis, P., & Plamondon, D. W. (2016, May). Compact modeling of data center raised-floor-plenum stanchions: Pressure drop through sparse tube bundles. In Thermal and Thermomechanical Phenomena in Electronic Systems (ITherm), 2016 15th IEEE Intersociety Conference on Thermal and Thermomechanical Phenomena in Electronic Systems, Las Vegas, NV, pp. 1148-1155.

[5]   Fulpagare, Y., Mahamuni, G., & Bhargav, A. (2015). Effect of plenum chamber obstructions on data center performance. Applied Thermal Engineering, (80), pp. 187-195.

[6]   Phan, L., Bhusal, S., & Lin, C. X. (2017, July). Improving cooling efficiency by using mixed tiles to control airflow uniformity of perforated tiles in a data center model. In ASME 2017 Heat Transfer Summer Conference, Bellevue, WA, pp. V001T08A005-V001T08A005.

[7]   Sharma, R. K., Bash, C. E. & Patel, C. D. (2002) Dimensionless parameters for evaluation of thermal design and performance of large-scale data centers. In: Presented at the 8th ASME/AIAA Joint Thermophysics and Heat Transfer Conference, St. Louis, MO, pp. 1–11.

[8]   Patel, C. D., Bash, C. E., Belady, C., Stahl, L. & Sullivan, D. (2001, July). Computational fluid dynamics modeling of high compute density data centers to assure system inlet air specifications. In Proceedings of IPACK conference, Kauai, HI, Vol. 1, pp. 8-13.

[9]   Cho, J. & Kim, B. S. (2011). Evaluation of air management system's thermal performance for superior cooling efficiency in high-density data centers. Energy and Buildings, 43(9), pp. 2145-2155.

[10]   Wang, X., Wang, X., Xing, G., Chen, J., Lin, C. X. & Chen, Y. (2013). Intelligent sensor placement for hot server detection in data centers. IEEE Transactions on Parallel and Distributed Systems, 24(8), pp. 1577-1588.

[11]   Sharma, R. K., Bash, C., Patel, C. D., Friedrich, R. & Chase, J. (2005) Balance of power: Dynamic thermal management for internet data centers. IEEE Internet Computing, 9(1), pp. 42–49.

[12]   Rambo, J. D. & Joshi, Y. K. (2003, January). Multi-scale modeling of high-power density data centers. In ASME 2003 International Electronic Packaging Technical Conference and Exhibition, Maui, HI, pp. 521-527.

[13]   Iyengar, M., Schmidt, R. R., Hamann, H. & VanGilder, J. (2007, January). Comparison between numerical and experimental temperature distributions in a small data center test cell. In ASME 2007 InterPACK Conference collocated with the ASME/JSME 2007 Thermal Engineering Heat Transfer Summer Conference, Vancouver, British Columbia, Canada, pp. 819-826.

[14]   Abdelmaksoud, W. A., Khalifa, H. E., Dang, T. Q., Schmidt, R. R. & Iyengar, M. (2010, June). Improved CFD modeling of a small data center test cell. In Thermal and Thermomechanical Phenomena in Electronic Systems (ITherm), Las Vegas, NV, pp. 1-9.

[15]   Abdelmaksoud, W. A., Dang, T. Q., Khalifa, H. E. & Schmidt, R. R. (2013). Improved computational fluid dynamics model for open-aisle air-cooled data center simulations. Journal of Electronic Packaging, 135(3), 030901.

[16]   Iyengar, M., Schmidt, R. R., Hamann, H. & VanGilder, J. (2007, January). Comparison between numerical and experimental temperature distributions in a small data center test cell. In ASME 2007 InterPACK Conference collocated with the ASME/JSME 2007 Thermal

FE-20-1718   Lin

Engineering Heat Transfer Summer Conference, Vancouver, British Columbia, Canada, pp. 819-826.

[17]   Abdelmaksoud, W. A., Khalifa, H. E., Dang, T. Q., Elhadidi, B., Schmidt, R. R. & Iyengar, M. (2010, June). Experimental and computational study of perforated floor tile in data centers. In Thermal and Thermomechanical Phenomena in Electronic Systems (ITherm), Las Vegas, NV, pp. 1-10.

[18]   Arghode, V. K. & Joshi, Y. (2014, May). Rapid modeling of air flow through perforated tiles in a raised floor data center. In IEEE Intersociety Conference on Thermal and Thermomechanical Phenomena in Electronic Systems (ITherm), Orlando, FL, pp. 1354-1365.

[19]   Arghode, V. K., Kumar, P., Joshi, Y., Weiss, T. & Meyer, G. (2013). Rack level modeling of air flow through perforated tile in a data center. Journal of Electronic Packaging, 135(3), 030902.

[20]   Phan, L., Hu, B. & Lin, C. X. (2019). An evaluation of turbulence and tile models at server rack level for data centers. Journal of Building and Environment (155), pp. 421 – 435.

[21]   Sirovich, L. (1987). Turbulence and the dynamics of coherent structures. I. Coherent structures. Quarterly of Applied Mathematics, 45(3), pp. 561-571.

[22]   Holland, J. H. (1992). Adaptation in natural and artificial systems: an introductory analysis with applications to biology, control, and artificial intelligence. MIT press.

[23]   Li, K., Xue, W., Xu, C. & Su, H. (2013) Optimization of ventilation system operation in office environment using POD model reduction and genetic algorithm.   Energy and Building (67), pp. 34 – 43.

[24]   Hu, W., Enying, L. & Yao, L. (2008) Optimization of sheet metal forming processes by adaptive response surface based on intelligent sampling method. Journal of Materials Processing Technology 197 (1-3) pp. 77– 88.

[25]   Egorov-Yegorov, I. N. & Dulikravich, G. S. (2005). Chemical composition design of superalloys for maximum stress, temperature, and time-to-rupture using self-adapting response surface optimization. Materials and Manufacturing Processes, 20(3), pp. 569-590.

[26]   Wang, G. G. (2003) Adaptive response surface method using inherited latin hypercube design points. ASME J. Mech. Des., 1 2 5, pp. 210–220.

[27]   Moral, R. & Dulikravich, G. S. (2008). A hybridized self-organizing response surface methodology. In 12th AIAA/ISSMO Multidisciplinary Analysis and Optimization Conference, Victoria, British Columbia, Canada, pp. 5891.

[28]   Box, G. E. & Wilson, K. B. (1951). On the experimental attainment of optimum conditions. Journal of the Royal Statistical Society: Series B (Methodological), 13(1), pp. 1-38.

[29]   Colaço, M. J., Dulikravich, G. S. & Sahoo, D. (2008). A response surface method-based hybrid optimizer. Inverse Problems in Science and Engineering, 16(6), pp. 717-741.

[30]   Colaço, M. J. & Dulikravich, G. S. (2008). A hybrid RBF based method for highly multidimensional response surfaces using scarce data sets. In 12th AIAA/ISSMO Multidisciplinary Analysis and Optimization Conference, Victoria, British Columbia, Canada, pp. 5892.

[31]   Dulikravich, G. S. & Colaco, M. J. (2015). Hybrid optimization algorithms and hybrid response surfaces. Chapter 2 in Advances in Evolutionary and Deterministic Methods for Design, Optimization and Control in Engineering and Sciences (eds.: D. Greiner, B. Galván, J. Periaux, N.

Gauger, K. Giannakoglou, G. Winter), Computational Methods in Applied Sciences Series, Springer Verlag, pp. 19-47.

[32]   Colaço, M. J. & Dulikravich, G. S. (2009). A survey of basic deterministic, heuristic and hybrid methods for single-objective optimization and response surface generation. Thermal Measurements and Inverse Techniques, 1, pp. 355-405.

[33]   Kansa, E. J., (1990) Multiquadrics – A Scattered Data Approximation Scheme with Applications to Computational Fluid Dynamics – II: Solutions to Parabolic, Hyperbolic and Elliptic Partial Differential Equations. Comput. Math. Appl., Vol. 19, pp. 149-161.

[34]   Hardy, R. L. (1971) Multiquadric Equations of Topography and Other Irregular Surfaces. Journal of Geophysics Res., Vol. 176, pp. 1905-1915.

[35]   Phan, L., Telusma, M., & Lin, C. X. (2015) Data center modeling using response surface with multiple-parameters approach. ASME 2015 International Mechanical Engineering Congress & Exposition, Houston, TX, USA, November 13 – 19.

[36]   Phan, L., & Lin, C. X. (2016) November). Multi-objective optimization of a data center modeling using response surface. In ASME 2016 International Mechanical Engineering Congress and Exposition, Phoenix, AZ, pp. V008T10A044-V008T10A044.

[37]   Launder, B. E., Spalding, D. B. (1974) The numerical computation of turbulent flows. Computer Methods in Applied Mechanics and Engineering, 3(2), pp. 269–289.

[38]   Jin, R., Chen, W. and Simpson, T. W. (2000) Comparative studies of metamodeling techniques under multiple modeling criteria. In Proceedings of the 8th AIAA/USAF/NASA/ISSMO Multidisciplinary Analysis & Optimization Symposium, AIAA 2000-4801, Long Beach, CA, September 6-8.

[39]   Sobol, I. M. (1976) Uniformly distributed sequences with an additional uniform property.

USSR Computational Mathematics and Mathematical Physics. (16), pp. 236–242.

[40]   ANSYS Inc., Fluent ver. 16.0. https://www.ansys.com/products/fluids/ansys-fluent

[41]   ESTECO S.R.L., modeFrontier ver. 450., Response surface training manual.

http://www.estecom.com/

List of Table Captions

FE-20-1718   Lin

Table 1. Choices for basis functions

Multiquadrics	$\phi(\lvert x - x_i \rvert) = \sqrt{(x - x_i)^2 + c_i^2}$	(11)
Inverse Multiquadrics	$\phi(\lvert x - x_i \rvert) = \dfrac{1}{\sqrt{(x - x_i)^2 + c_i^2}}$	(12)
Gaussian	$\phi(\lvert x - x_i \rvert) = e^{-c(x - x_i)^2}$	(13)
Polyharmonic splines	$\phi(\lvert x - x_i \rvert) = \begin{cases} (x - x_i)^{2n} \log(x - x_i), n \geq 1, & in\ 2D \\ (x - x_i)^{2n-1}, \ n \geq 1, & in\ 3D \end{cases}$	(14)

Table 2. Summary table for the attributes of the genetic algorithm used during the optimization

process

Number of design variables (T_1, T_2, ..., T_8)	8
Initial population size	45
Number of generations	100
Probability of Mutation	1.5%
Probability of Elitism	3%
Probability of directional crossover	50%

FE-20-1718   Lin

Table 3. Initial designs for response surface construction

Cases	Tile Porosity							
	Tile 1	Tile 2	Tile 3	Tile 4	Tile 5	Tile 6	Tile 7	Tile 8
1	0.28	0.63	0.63	0.63	0.28	0.28	0.63	0.28
2	0.63	0.28	0.28	0.28	0.63	0.63	0.28	0.63
3	0.71	0.71	0.19	0.36	0.71	0.54	0.71	0.36
4	0.36	0.36	0.54	0.71	0.36	0.19	0.36	0.71
5	0.19	0.54	0.36	0.19	0.19	0.36	0.54	0.54
6	0.54	0.19	0.71	0.54	0.54	0.71	0.19	0.19
7	0.58	0.67	0.41	0.76	0.14	0.67	0.76	0.41
8	0.23	0.32	0.76	0.41	0.49	0.32	0.41	0.76
9	0.41	0.49	0.23	0.58	0.67	0.14	0.58	0.58
10	0.76	0.14	0.58	0.23	0.32	0.49	0.23	0.23

FE-20-1718   Lin

Table 4. RBF performance assessment for 4 different stages

Functions	RAAE	RMAE	R-squared
Multiquadrics	0.098	1.018	0.934
Gaussians	0.379	1.148	0.789
Inverse Multiquadrics	0.111	1.215	0.915
Polyharmonic Splines	0.114	1.589	0.909

a) Stage 1

Functions	RAAE	RMAE	R-squared
Multiquadrics	0.061	0.706	0.977
Gaussians	0.108	1.444	0.913
Inverse Multiquadrics	0.067	0.825	0.971
Polyharmonic Splines	0.109	1.842	0.901

b) Stage 2

Functions	RAAE	RMAE	R-squared
Multiquadrics	0.034	0.364	0.994
Gaussians	0.071	1.258	0.961
Inverse Multiquadrics	0.036	0.472	0.993
Polyharmonic Splines	0.068	0.954	0.967

c) Stage 3

Functions	RAAE	RMAE	R-squared
Multiquadrics	0.028	0.311	0.996
Gaussians	0.099	0.921	0.951
Inverse Multiquadrics	0.031	0.314	0.996
Polyharmonic Splines	0.048	0.736	0.987

d) Stage 4

FE-20-1718   Lin

Table 5. Targeted tile mass flow rate distribution at different shapes

Tile ID	Tile Mass Flow Distribution (kg/s)								Total Mass Flow (kg/s)
	1	2	3	4	5	6	7	8	
Scenario 1 (Linear)	0.66	0.90	1.14	1.38	1.62	1.86	2.10	2.34	12.0
Scenario 2 (Parabolic)	2.70	1.67	0.99	0.64	0.64	0.99	1.67	2.70	12.0
Scenario 3 (Sinusoidal)	0.50	2.50	0.50	2.50	0.50	2.50	0.50	2.50	12.0

FE-20-1718   Lin

Table 6. Total time comparison for the whole design process between CFD and RSM methods.

Tasks	Design optimization without RSM	Design optimization with RSM
Original data set	45 cases x 2 hrs./case = 90 hours	45 cases x 2 hours/case = 90 hrs.
Optimization process	4500 designs x 2hrs/design = 9000 hrs.	RSM training: a few seconds 4 stages x 10 cases/stage x 2 hrs./case = 80 hrs.
Total	~9090 hrs. or ~379 days	~ 170 hrs. or ~ 7 days

FE-20-1718   Lin

List of Figure Captions

Fig. 1. A simplified data center overview floor plan with floor tiles shown

FE-20-1718   Lin
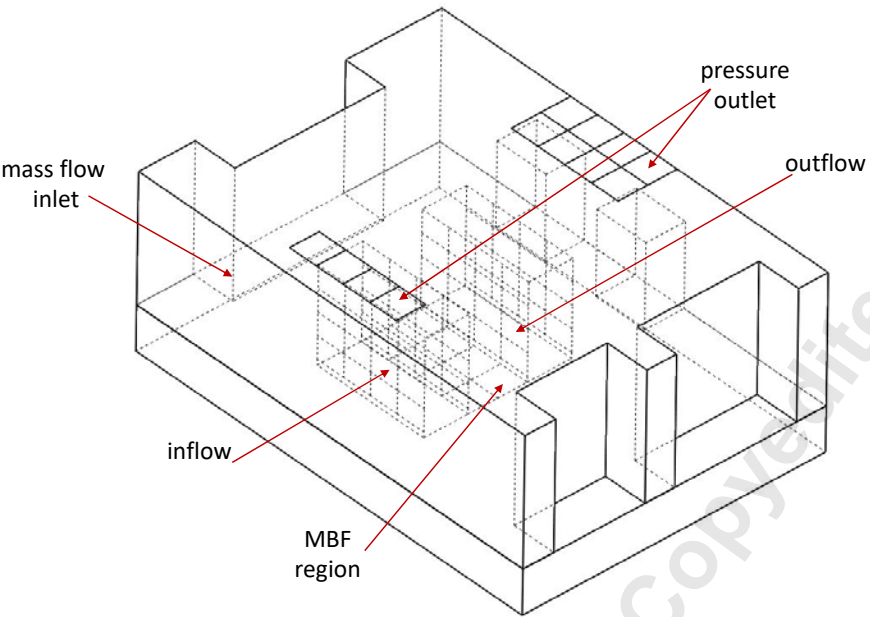
Fig. 2. Computational domain and boundary conditions
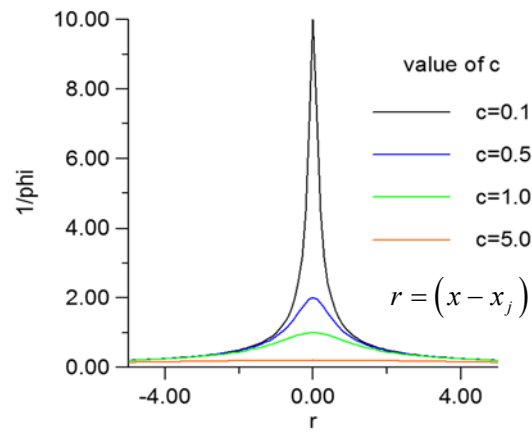
Fig. 3. The influence of shape parameter c_j on multiquadrics RBF [32]

FE-20-1718   Lin

a) Multiquadrics

b) Inverse Multiquadrics

c) Gaussians

d) Polyharmonic Splines
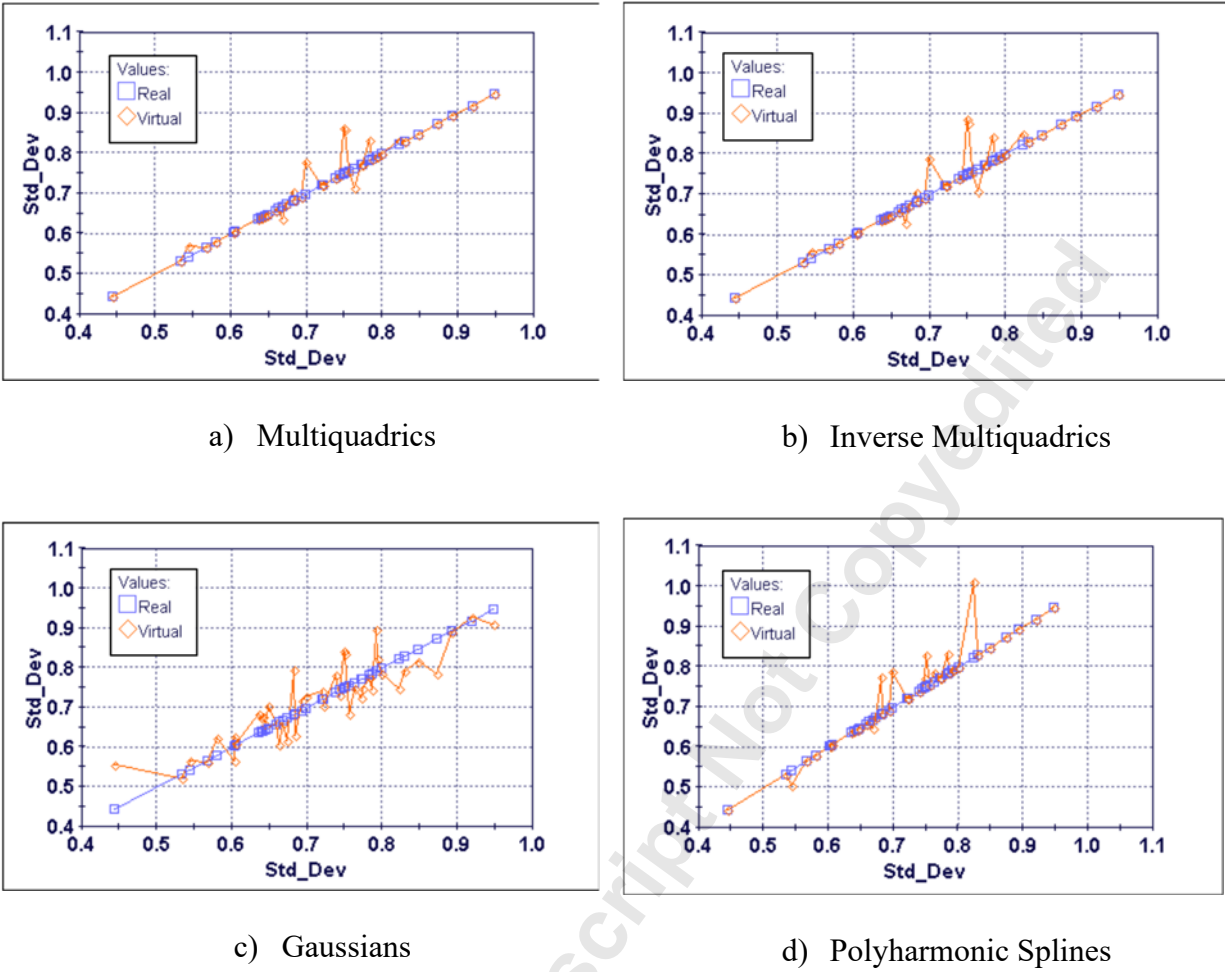
Fig. 4. Distance chart between real designs by CFD and virtual designs by RSM in the 1st stage

43   FE-20-1718   Lin
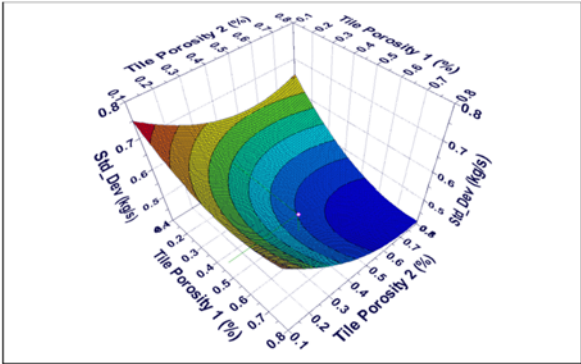
a) 3D response surface of the standard deviation
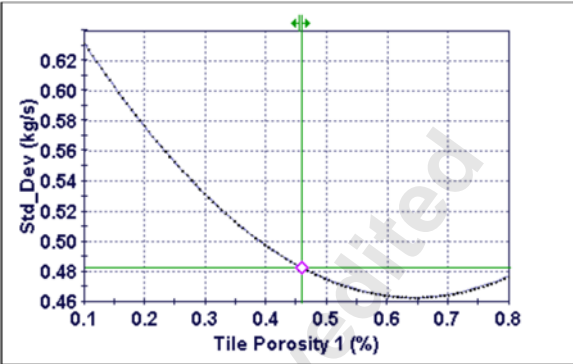
b) Standard deviation vs. tile 1 porosity
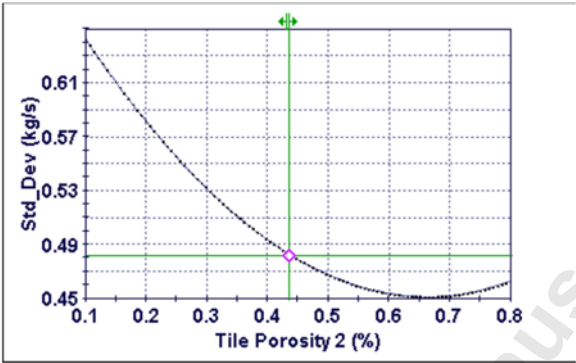
c) Standard deviation vs. tile 2 porosity
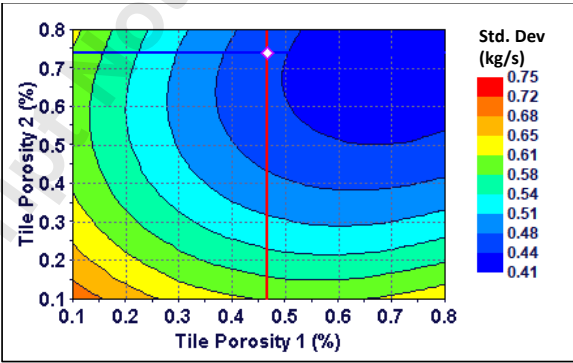
d) Tile 2 porosity vs. tile 1 porosity

Fig. 5. 3D response surface exploration for *multiquadrics* in the 1st stage

FE-20-1718   Lin

a) Stage 1

b) Stage 2

c) Stage 3

d) Stage 4
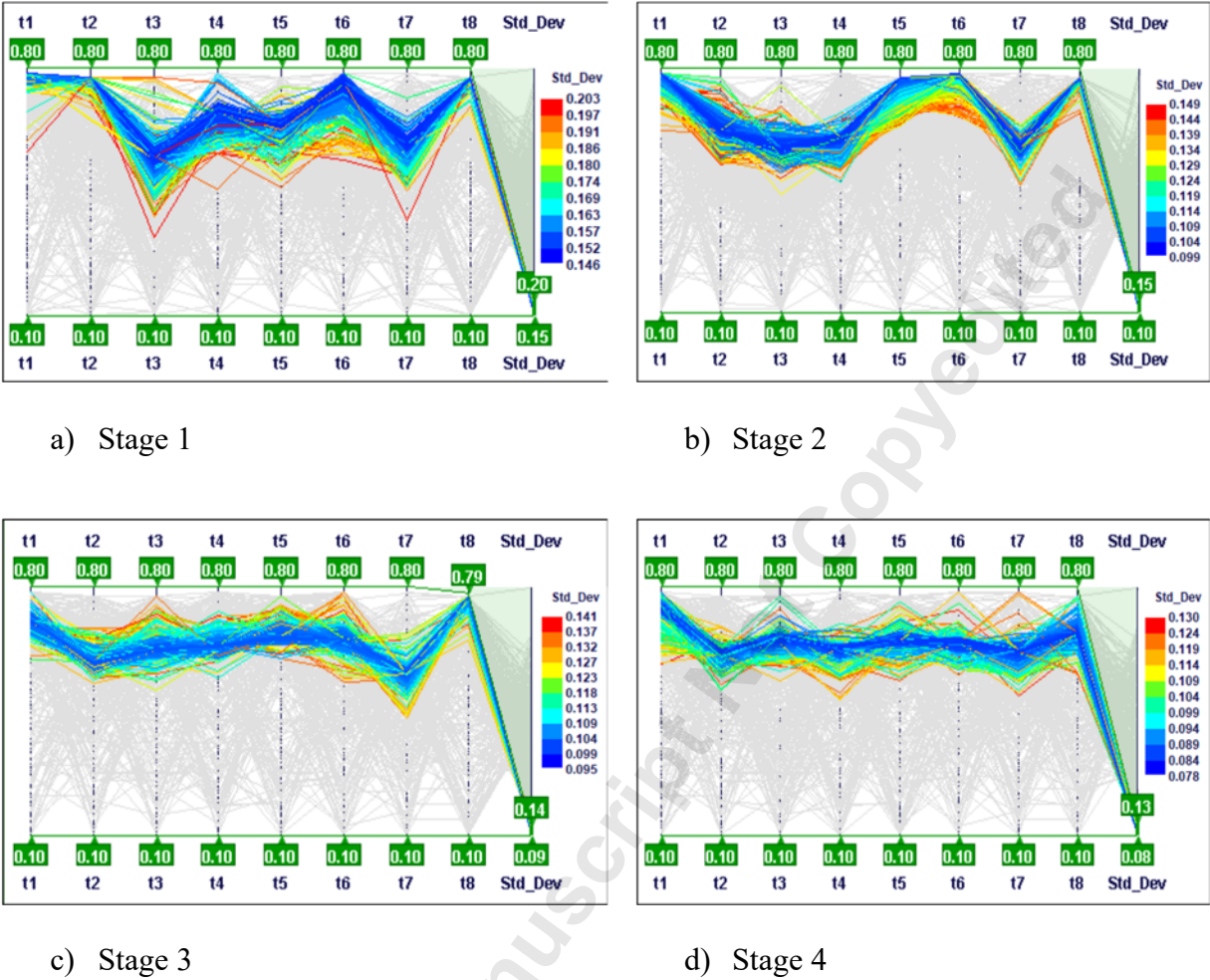
Fig. 6. Optimum tile porosity combinations for minimum standard deviation objective at

different stages
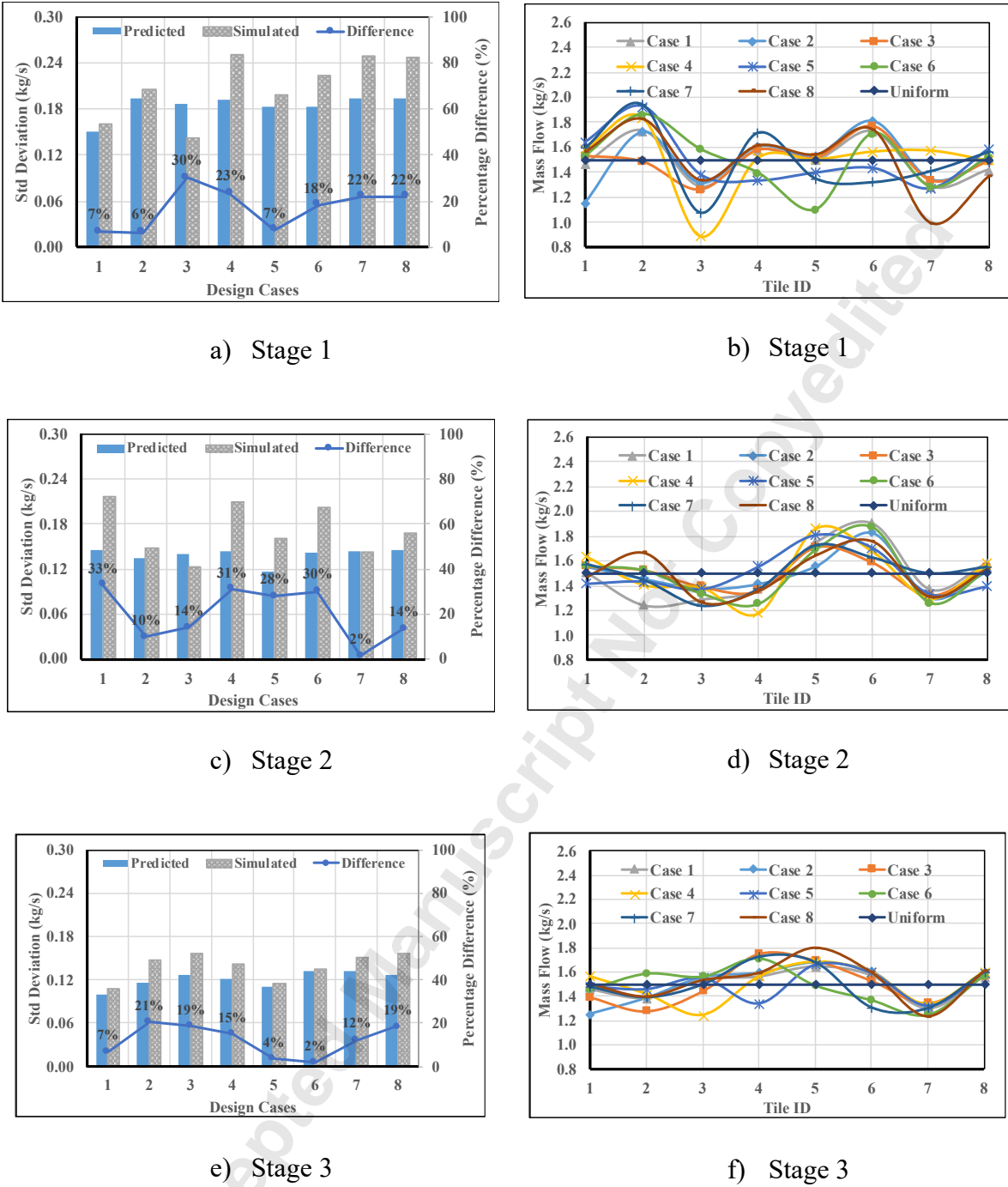
FE-20-1718   Lin

a) Stage 1

b) Stage 1

c) Stage 2

d) Stage 2

e) Stage 3

f) Stage 3

Fig. 7. Design validation via stages: a), c), e) Comparison of the tile mass flow rate

standard deviation between the predicted RSM and the simulated CFD values. b), d), f) The

simulated CFD values of tile mass flow rate for cases validated at each stage
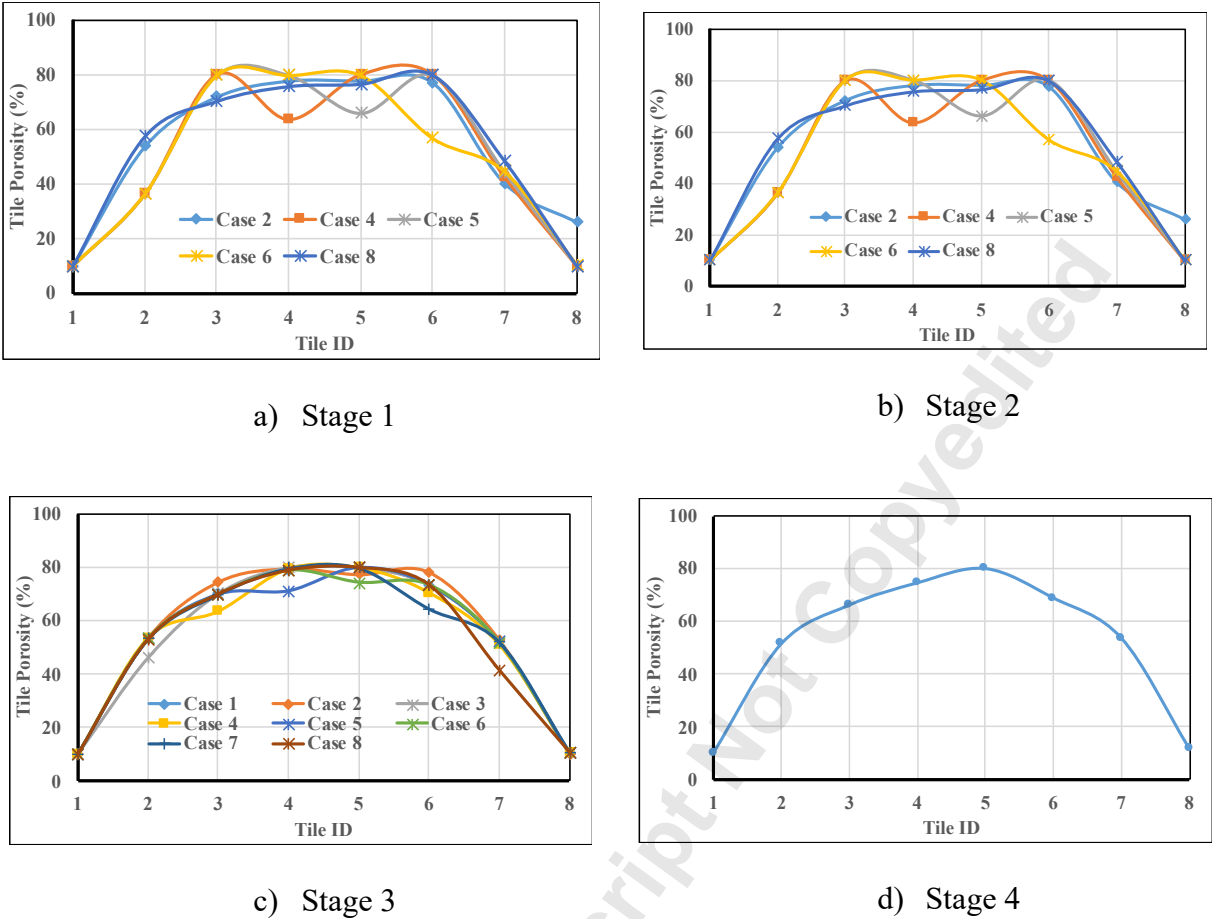
FE-20-1718 Lin

a) Stage 1

b) Stage 2

c) Stage 3

d) Stage 4
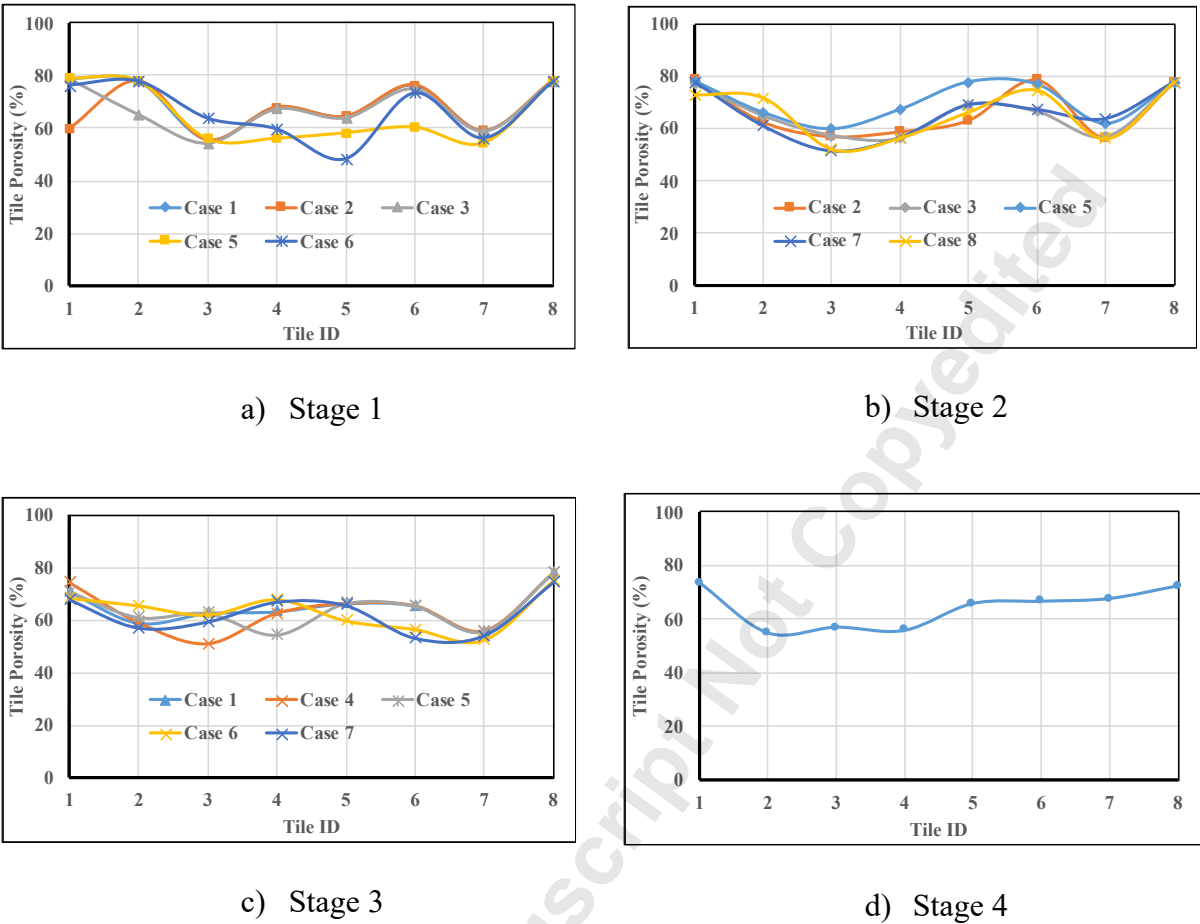
Fig. 8. Tile porosity for best-validated designs at each stage

FE-20-1718   Lin
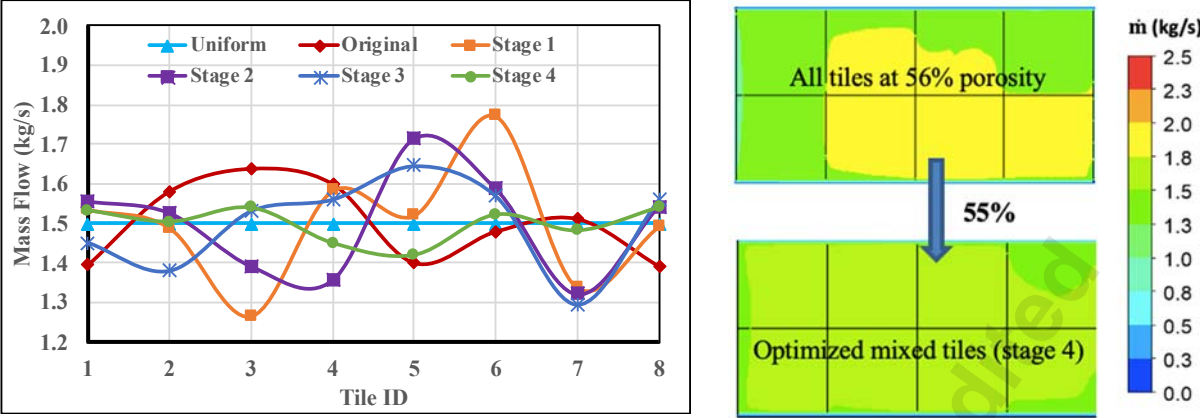
a)   Tile mass flow rate for all best designs at each

stage compared to the original and uniform

cases

b) Relative tile airflow

uniformity improvement

Fig. 9. Tile mass flow rate comparison

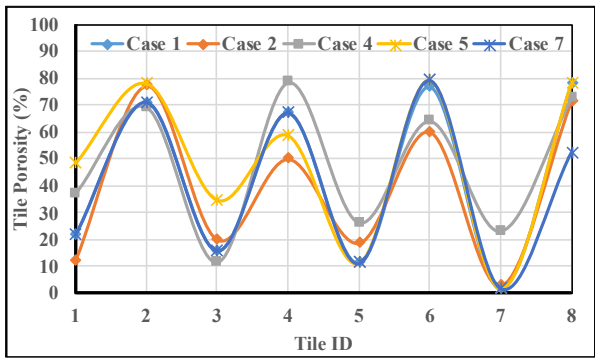FE-20-1718   Lin
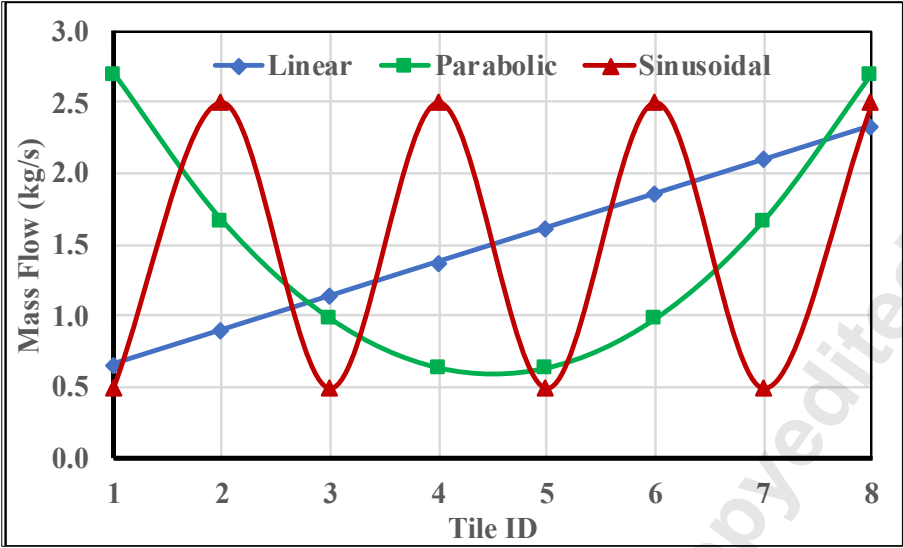
Fig. 10. Targeted shape for different tile mass flow rate distribution

a)   Stage 1

b)   Stage 2

c)   Stage 3

d)   Stage 4
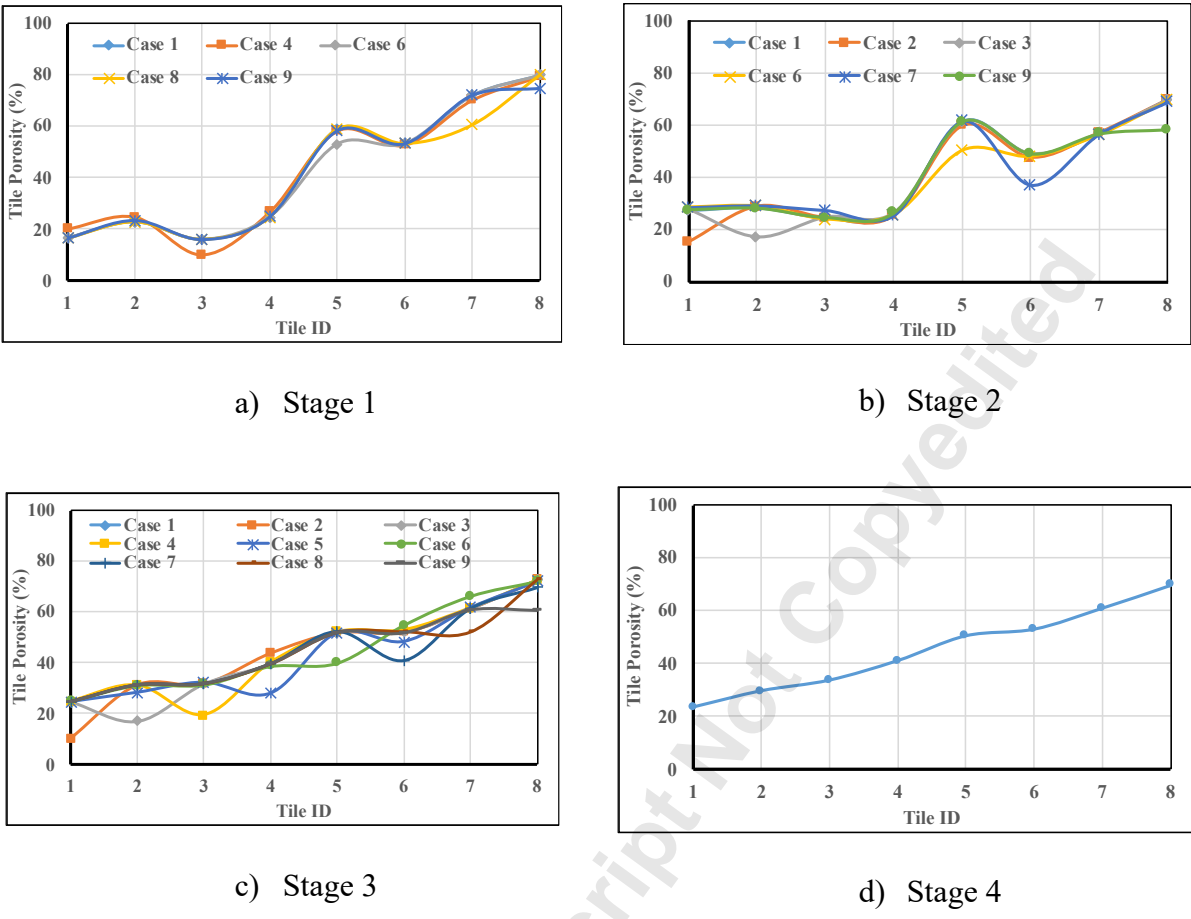
Fig. 11. Tile porosity for best-validated designs at each stage

FE-20-1718   Lin
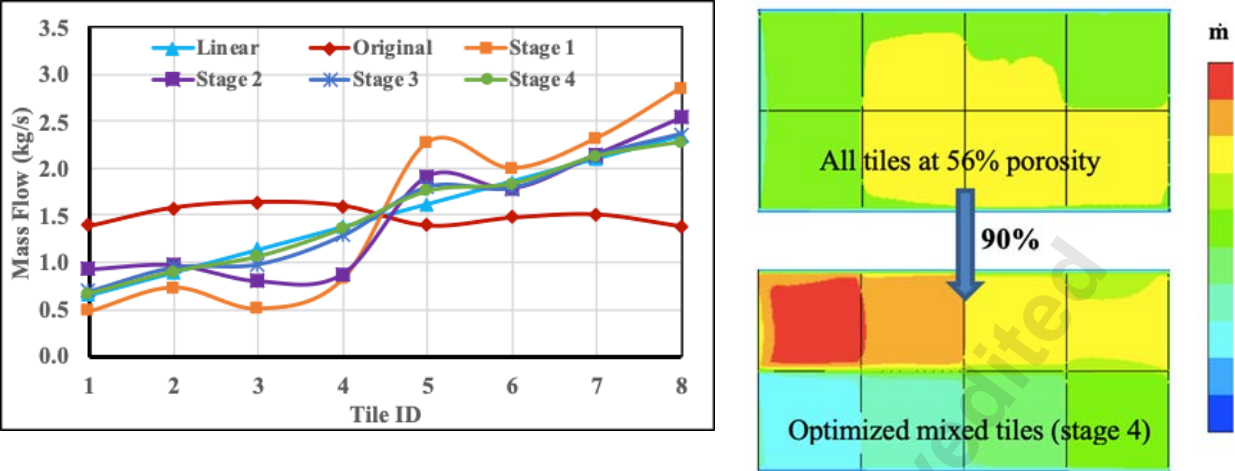
a) Tile mass flow rate for all best designs at each

stage compared to the original and proposed

linear airflow distribution designs

b) Relative tile airflow
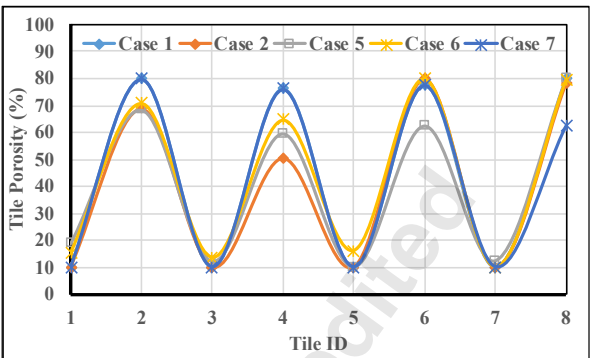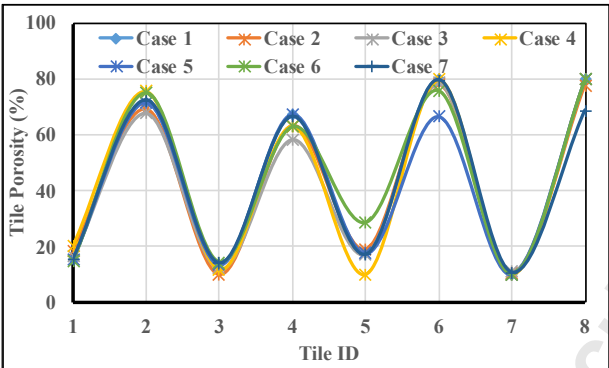
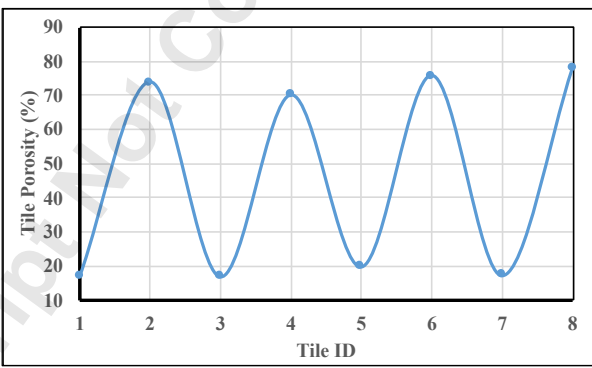uniformity improvement

Fig. 12. Tile mass flow rate comparison

a) Stage 1

b) Stage 2

c) Stage 3

d) Stage 4

Fig. 13. Tile porosity for best-validated designs at each stage

a) Tile mass flow rate for all best designs at each

stage compared to the original and uniform

cases

b) Relative tile airflow

uniformity improvement
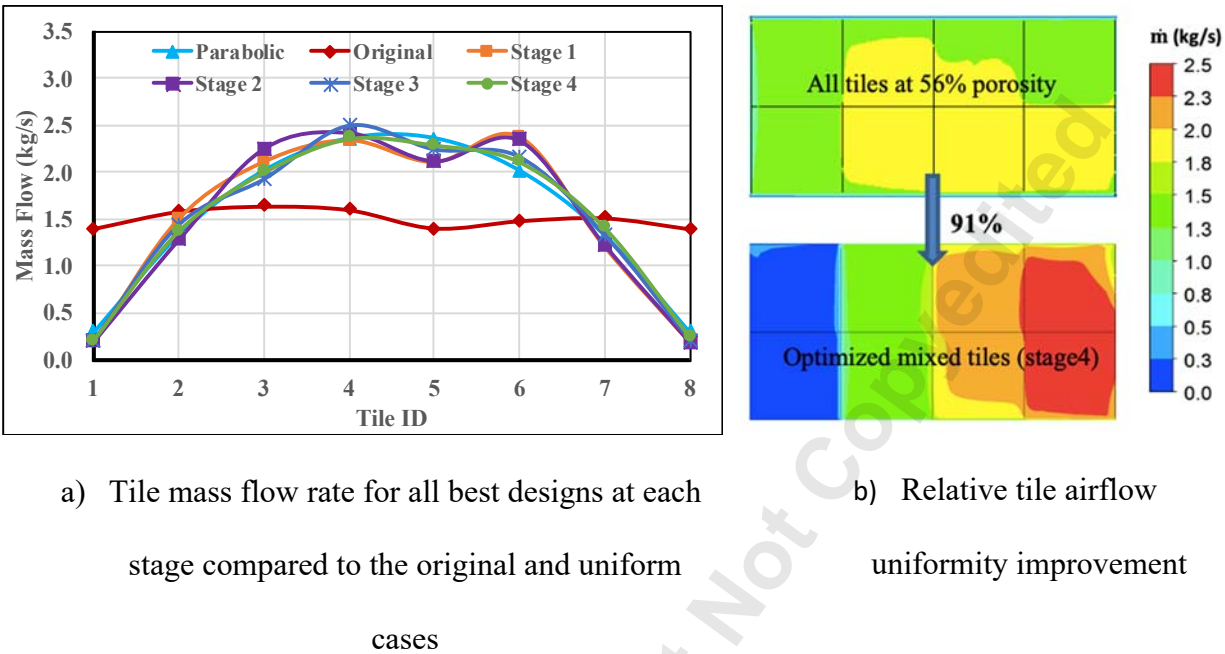
Fig. 14. Tile mass flow rate comparison

a) Stage 1

b) Stage 2

c) Stage 3

d) Stage 4

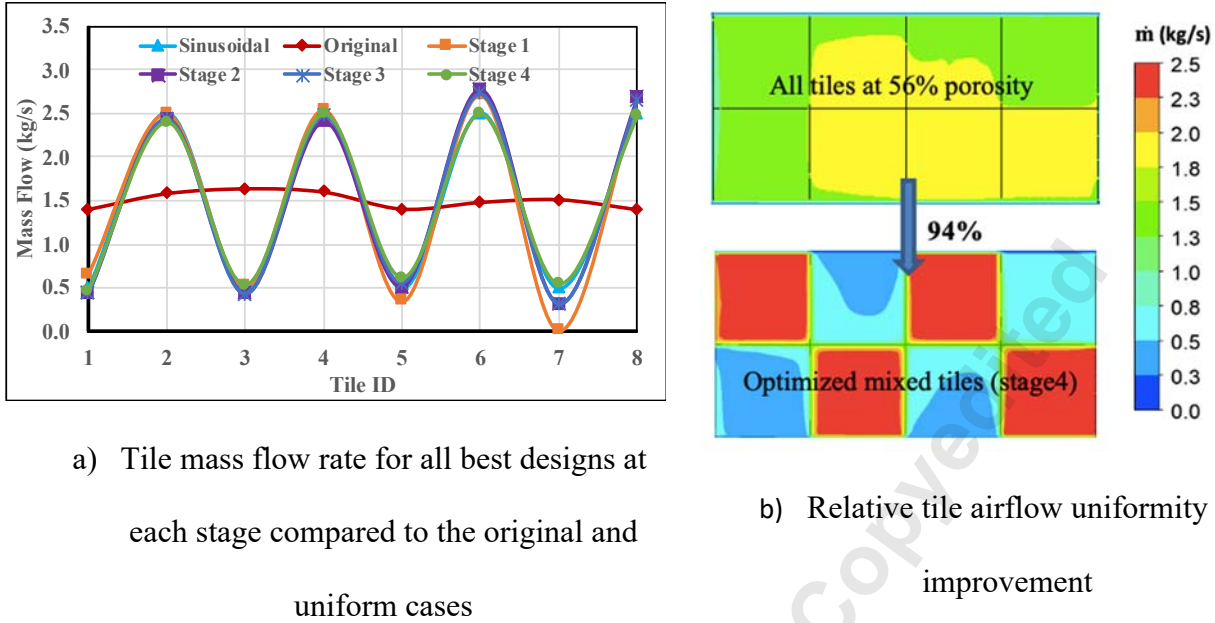Fig. 15. Tile porosity for best-validated designs at each stage

a) Tile mass flow rate for all best designs at

each stage compared to the original and

uniform cases

b) Relative tile airflow uniformity

improvement

Fig. 16. Tile mass flow rate comparison

FE-20-1718   Lin

APPENDIX

Linear tile airflow distribution

a)   Stage 1

b)   Stage 2

c)   Stage 3

d)   Stage 4

Fig. 17. Optimal designs sort out at different stages

a) Stage 1

b) Stage 1

c) Stage 2

d) Stage 2
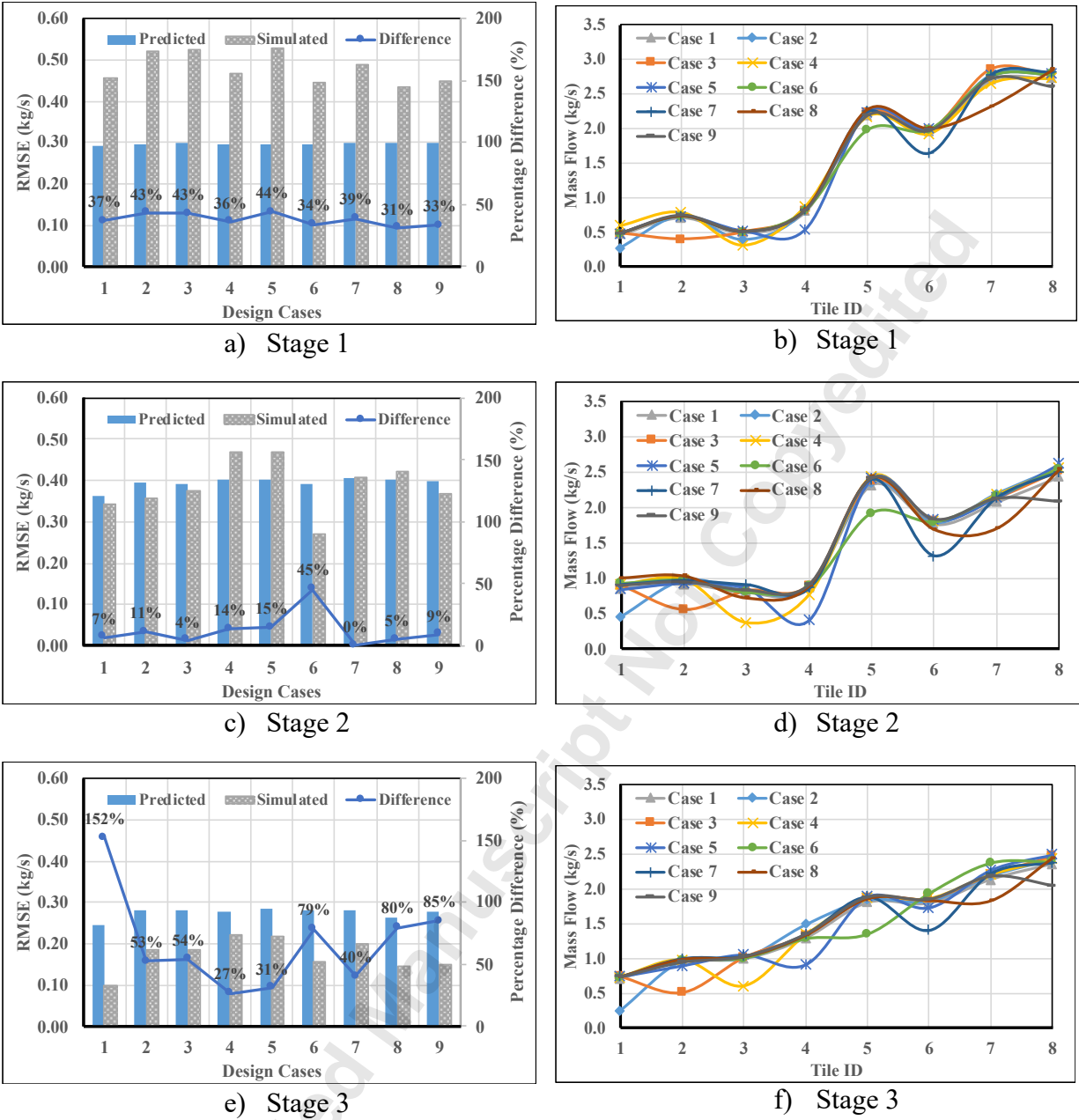
e) Stage 3

f) Stage 3
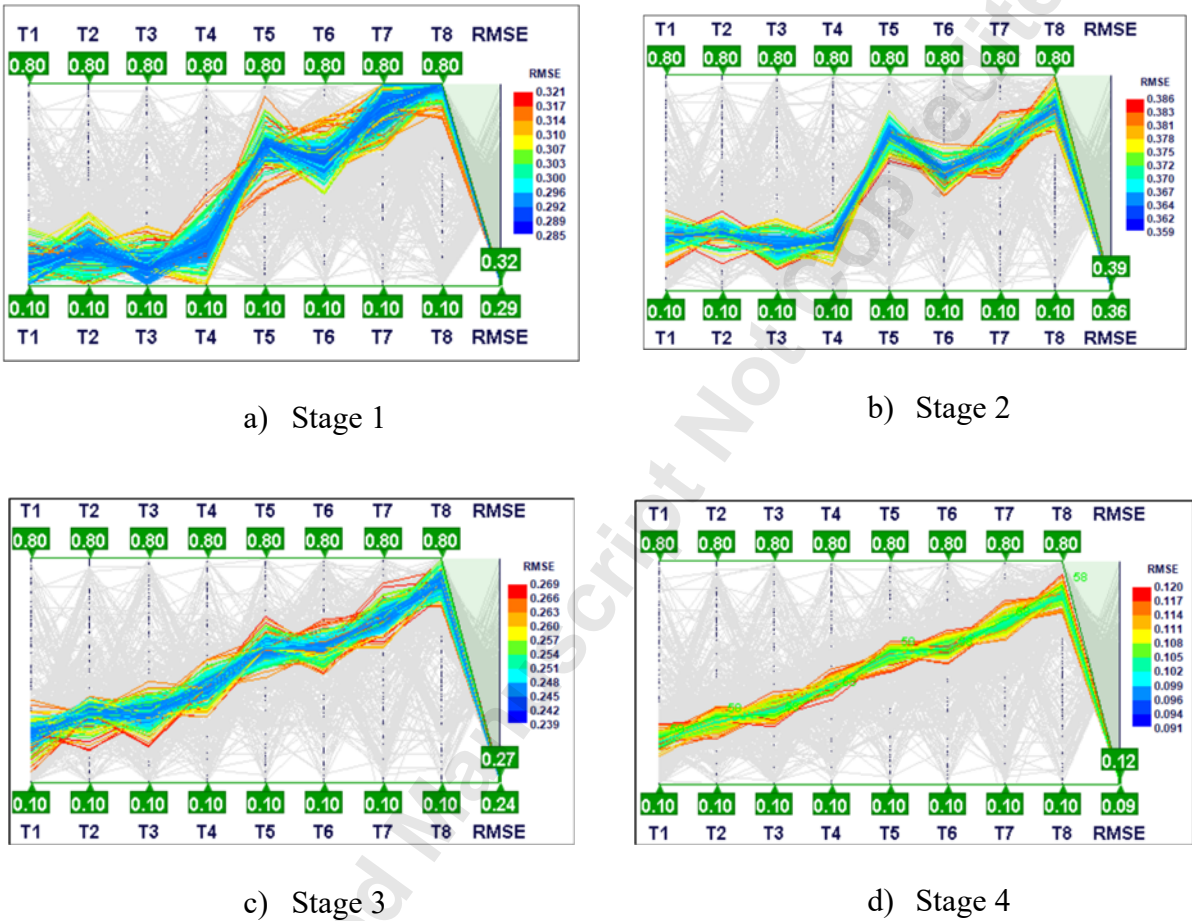
Fig. 18. Designs validation via stages: a), c), e) Comparison of the tile mass flow rate standard

deviation between the predicted RSM and the simulated CFD values. b), d), f) The simulated

CFD values of tile mass flow rate for cases validated at each stage

Parabolic tile airflow distribution

Fig. 19. Optimal designs sort out at different stages

a) Stage 1

b) Stage 1

c) Stage 2

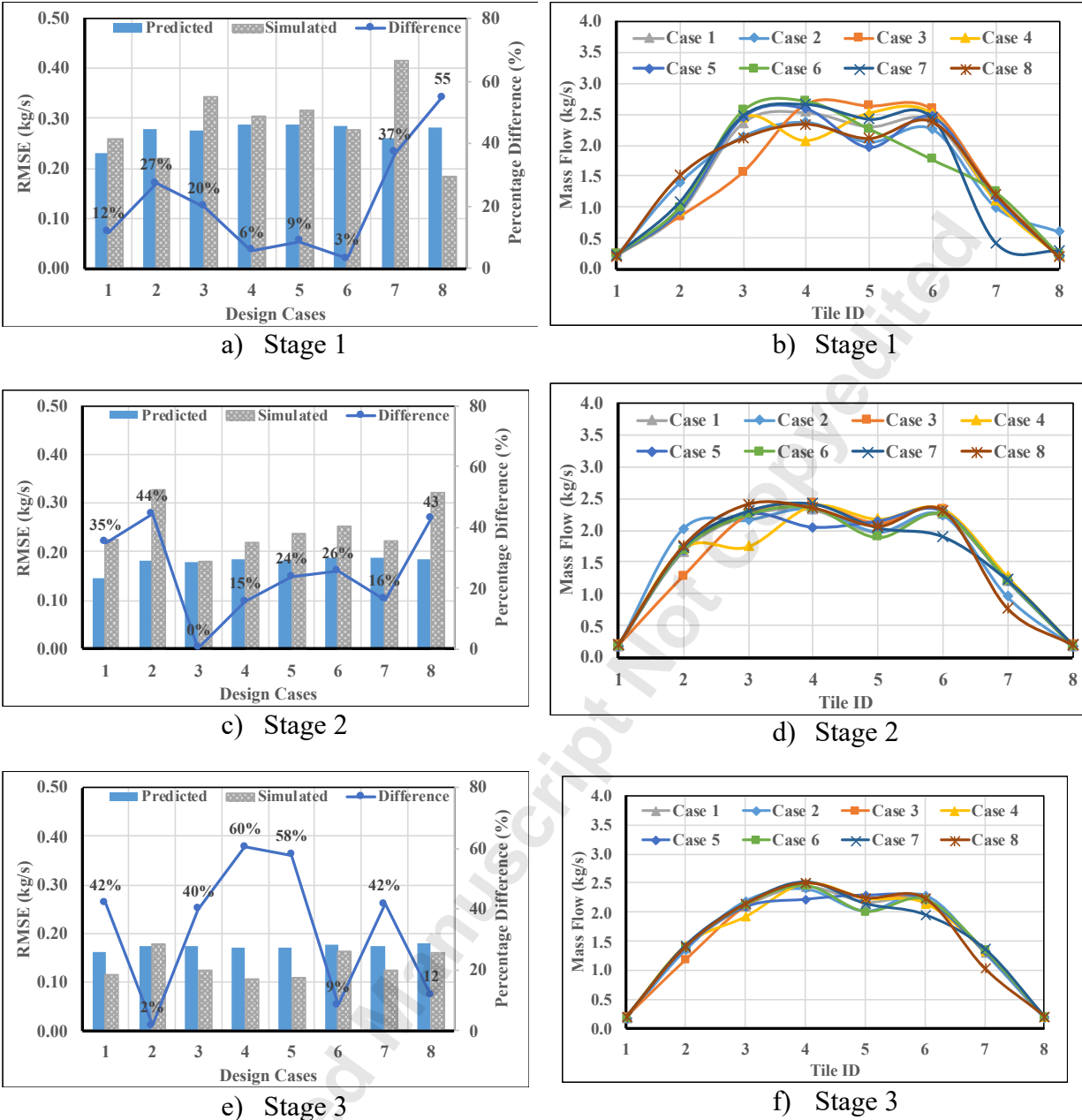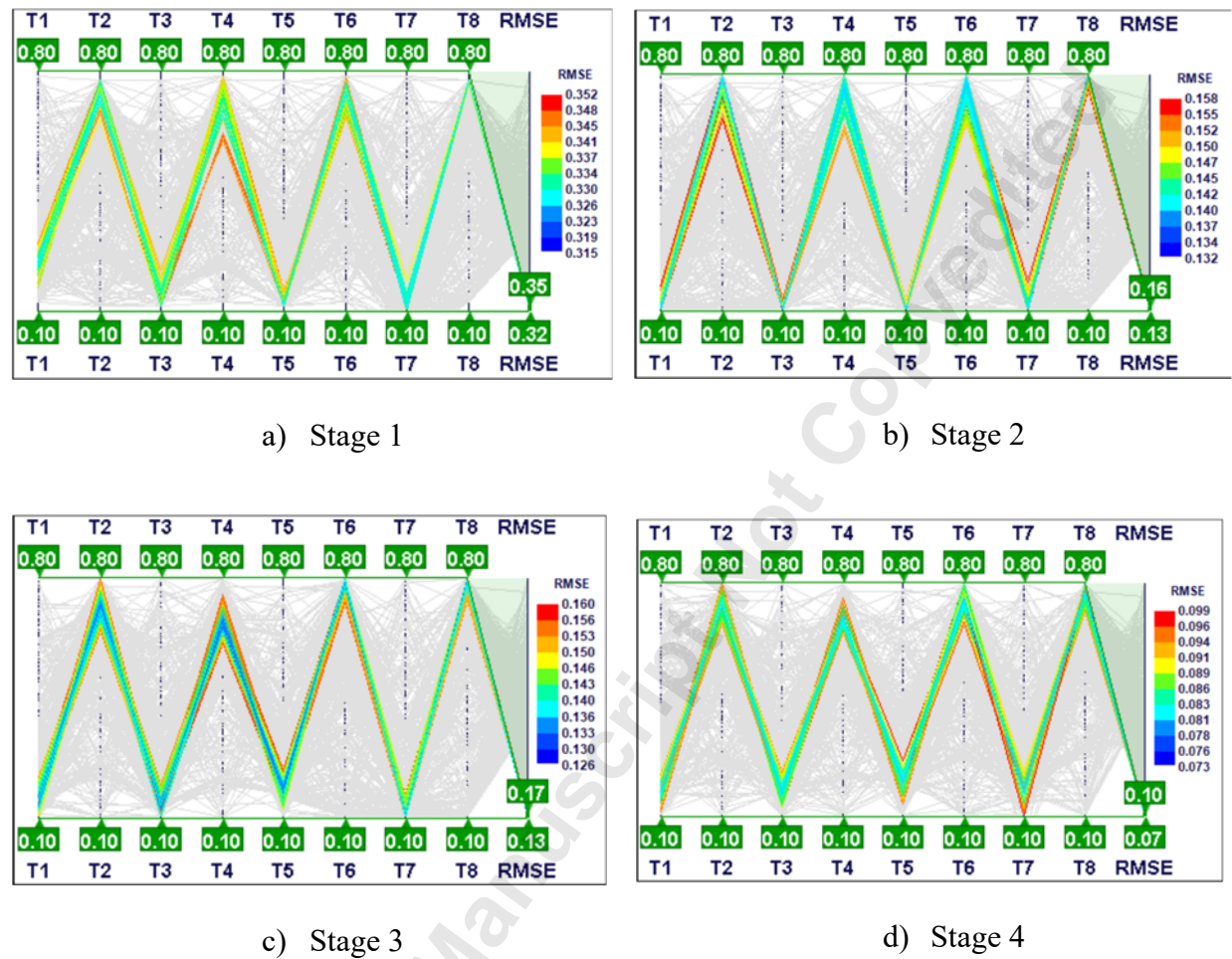d) Stage 2

e) Stage 3

f) Stage 3

Fig. 20. Design validation via stages: a), c), e) Comparison of the tile mass flow rate standard

deviation between the predicted RSM and the simulated CFD values. b), d), f) The simulated

CFD values of tile mass flow rate for cases validated at each stage

FE-20-1718   Lin

Sinusoidal tile airflow distribution

a) Stage 1

b) Stage 2

c) Stage 3

d) Stage 4

Fig. 21. Optimal designs sort out at different stages

FE-20-1718   Lin

a) Stage 1   b) Stage 1
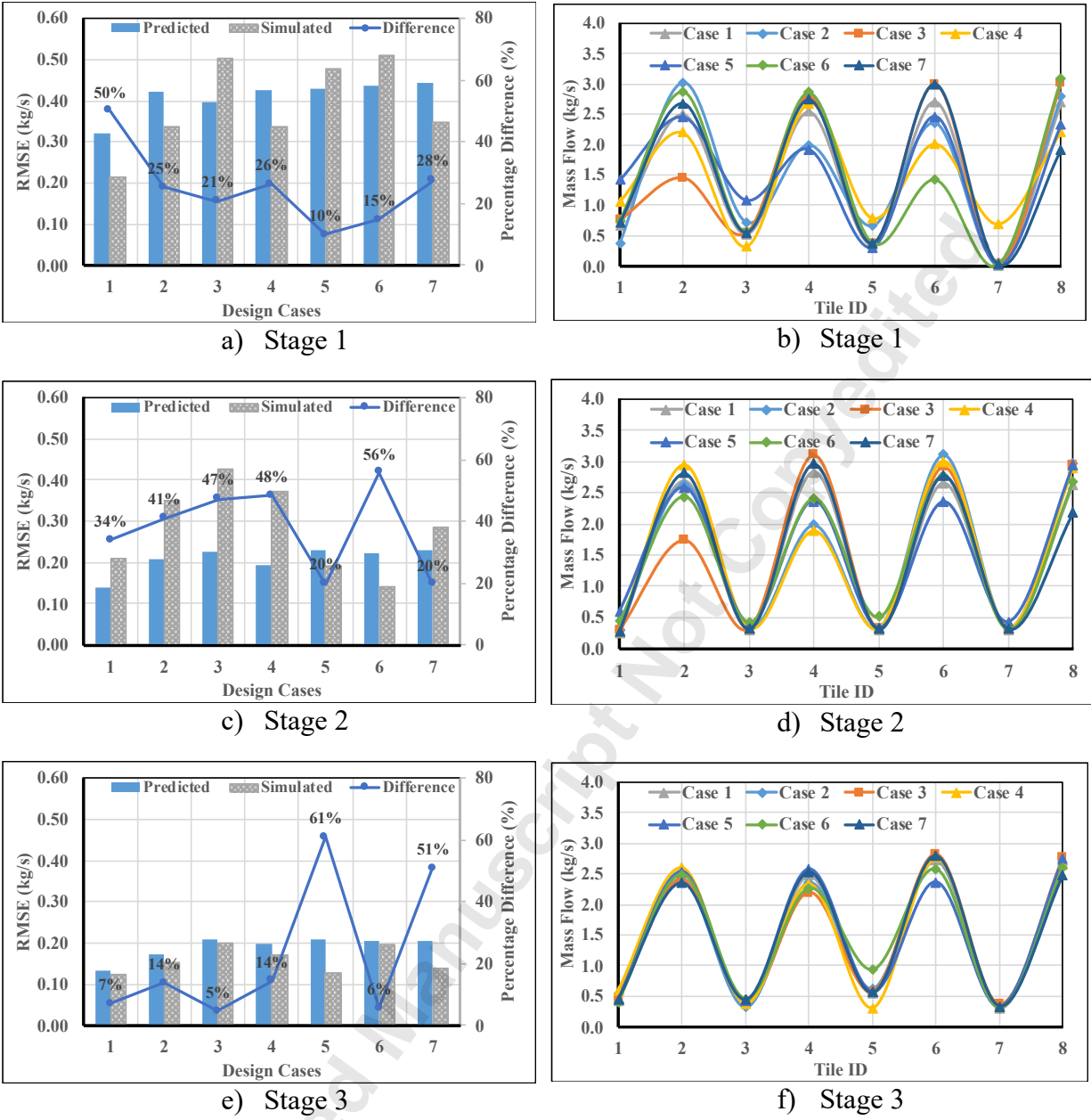
c) Stage 2   d) Stage 2

e) Stage 3   f) Stage 3

Fig. 22. Design validation via stages: a), c), e) Comparison of the tile mass flow rate standard

deviation between the predicted RSM and the simulated CFD values. b), d), f) The simulated

CFD values of tile mass flow rate for cases validated at each stage

Highlights

- Response surface based optimization allows thousands of candidate designs to be generated cheaply

- Radial basis function shows a fast-approximation technique in response surface construction

- Airflow uniformity through tiles is achieved through optimization of mixed-porosity tiles arrangement

- A specific tile airflow distribution is attainable for non-uniform thermal loading within server racks

FE-20-1718   Lin